GLOBAL MODELS OF PULSE-POWER MODULATED HIGH DENSITY, LOW PRESSURE DISCHARGES

by

M. A. Lieberman and S. Ashida

Memorandum No. UCB/ERL M95/83

20 October 1995

GLOBAL MODELS OF PULSE-POWER MODULATED HIGH DENSITY, LOW PRESSURE DISCHARGES

by

M. A. Lieberman and S. Ashida

Memorandum No. UCB/ERL M95/83

20 October 1995

ELECTRONICS RESEARCH LABORATORY

College of Engineering
University of California, Berkeley
94720

GLOBAL MODELS OF PULSE-POWER MODULATED HIGH DENSITY, LOW PRESSURE DISCHARGES

M.A. Lieberman

Department of Electrical Engineering and Computer Sciences
and the Electronics Research Laboratory
University of California
Berkeley, CA 94720-1770 USA

and

S. Ashida

Materials and Devices Research Laboratories
Toshiba Corporation
Yokohama 235 Japan

ABSTRACT

Global (volume-averaged) models of high density, low pressure electropositive and electronegative discharges are described for both continuous wave (cw) and pulsed-power excitation. Argon and chlorine discharges are treated. The particle and energy balance equations are applied to determine the charged particle and neutral dynamics. For argon just after the power is turned on, the analysis shows an initial very sharp rise in electron temperature T_e, followed by a decay of T_e and an increase in the electron density n_e to steady state values during the pulse on-time. Just after the power is turned off, T_e decays rapidly and n_e decays more slowly. The time-average n_e can be considerably higher than that for cw discharges for the same time-average power. For chlorine, a cw discharge is highly dissociated and the negative ion density n_{Cl^-} is lower than n_e. For a pulsed discharge, the initial rise and subsequent decay of n_{Cl^-} just after the power is turned off are determined analytically. A pulsed discharge can have the same neutral radical (Cl) flux to the walls for a reduced average power. The analytical models are compared to more complete global model simulations and to experimental observations. We find that global models can provide considerable insight into the discharge dynamics.

I. INTRODUCTION

High density, low pressure plasma sources utilizing modulated power have been attracting much attention recently. High density sources, such as electron cyclotron resonance discharges (ECR's), inductively coupled plasmas (ICP's), and helicons are regarded as powerful tools that can replace conventional capacitively coupled, parallel plate plasma reactors. A major advantage is that much higher manufacturing throughput can be expected because much higher plasma densities than those of parallel plate reactors are obtainable. Another advantage is that aspect ratio-independent anisotropic etch processes are possible because of lower gas pressures. It is also a great advantage that the ion bombarding energy can be controlled independently of the ion flux. By modulating the power, it is possible to further optimize and control the performance of processing plasmas by changing the pulse frequency and duty ratio.

Samukawa and Furuoya[1] and Samukawa[2] reported that the etch selectivity of silicon against SiO_2 was greatly improved by controlling the duty ratio of the pulsed microwave power supplied to a CHF_3 ECR source. Samukawa[3] has also shown that vertical and notch-free polycrystalline etching profiles can be achieved in pulsed Cl_2 ECR discharges by controlling the ion energy distributions through the duty ratio, and Samukawa and Terada[4] have shown that charge build-up damage can also be controlled in pulsed Cl_2 and O_2 ECR discharges. Mieno and Samukawa[5] attribute polysilicon etching and a reduction in charge accumulation on the substrate to the flux of negative ions incident on the substrate in the afterglow (off-time of power application) of a pulsed Cl_2 ECR discharge.

Charles and Boswell[6] studied pulsed O_2 helicon discharges used for deposition of SiO_2 films. They showed that the ion flux and energy distribution can be significantly modified by pulsing the discharge. Charles et al[7] showed that the SiO_2 deposition rate and the heat load on the substrate could be controlled by varying the pulsing frequency in an O_2/SiH_4 helicon diffusion plasma.

Wendt et al[8] showed that extended pressure and power operation ranges were possible in pulsed operation of a planar ICP plasma source. Sugai et al[9] showed that the density ratio of CF_x/F in a CF_4/H_2 ICP pulsed discharge increases with decreasing rf on-time and that highly selective SiO_2/Si etching could be achieved only with pulsed operation.

Ahn et al[10] measured the negative ion density in a pulsed Cl_2 ICP discharge and showed the presence of a large negative ion density in the afterglow. Shindo and Horiike[11] showed that silicon is etched by low energy F^- ions even at cryogenic temperatures where F atom etching of silicon is suppressed. Hollenstein et al[12] suggest that particulate formation can be suppressed by pulsing the discharge to periodically remove negatively charged particle precursors; e.g., high molecular weight negative ions. Nogami et al[13] observed the same SiO_2 etch rate for pulsed and cw discharges with the same average power.

As reported in almost all of these references, pulsed argon discharges have been operated and used as a benchmark and to contrast to results obtained in reactive electronegative discharges such as Cl_2, O_2, CHF_3, etc. For example, Ashida et al[14], Sugai et al[9], and Ahn et al[10] used Langmuir probes to determine time-varying plasma density and electron temperature in pulsed ICP discharges.

Few theoretical analyses of high density, low pressure pulsed operation have been published. Such analyses may give us a fundamental understanding of mechanisms governing processes and thus help us design better reactors, and find suitable modulation periods and various other parameters. Ashida et al[15] investigated the behavior of argon plasmas driven by time modulated power in high density plasma reactors using a spatially averaged (global) model. The time evolution of the electron temperature and the plasma density was calculated by solving the particle and energy balance equations. The species considered in the model included ground state Ar, 4s (resonance and metastable) excited Ar, 4p excited Ar, and Ar^+ ions. For typical pressures and absorbed powers, the excited Ar states affected the calculated plasma density by at most 25% and had practically no effect on the electron temperature. It was found that much higher plasma densities can be obtained by selecting an appropriate modulation period, than when operating with continuous power, for the same time-average input power. The global model gives much simpler equations than simulation methods such as particle-in-cell (PIC)[16] or fluid models[17,18]. Therefore, this model does not require much computational resources. Moreover, the equations are so simple that the relations between fundamental mechanisms and resulting plasma parameters become clear. A simplified global model (without excited states) is described in Sec. II, and comparisons with measurements are given.

Although pulsed power argon discharges are useful benchmarks, electronegative discharges are used for most materials processing applications. A simplified global model for pulsed power electronegative discharges such as O_2 or Cl_2 is presented in Sec. III. For high density, low pressure discharges, it is shown that the electronegativity (ratio of negative-ion to electron density) is typically less than unity during the on-time of the power pulse, but can grow rapidly to a value exceeding unity during the off-time (the afterglow). We compare the simple model predictions with experiments in Sec. III. A more complete global model of high density pulsed Cl_2 discharges is given by Ashida and Lieberman[19]. Low density capacitively coupled pulsed discharges are beyond the scope of the present study; the reader is referred to Overzet and Leong-Rousey[20] and the references cited therein.

II. ELECTROPOSITIVE DISCHARGES

A. Steady State Model

The pulsed power argon (electropositive) discharge model is based on the steady state model of Lee et al[21,22] for a cylindrical plasma discharge of radius R and length L. The model assumes uniform spatial distributions of plasma parameters over the volume of a bulk plasma, with the plasma density n_e in the bulk dropping sharply to edge values n_{sL} and n_{sR} at the thin sheaths close to the axial and circumferential walls. Electron-ion pairs are assumed to be created by electron-impact ionization of the background gas and are lost by diffusive flow to the walls. Two step and metastable-metastable ionization is neglected. It is also assumed that the plasma is electrically neutral and that the ion and electron fluxes toward the walls balance at all times; ie, that the flow is ambipolar. For the low pressures of interest, the characteristic diffusive flow velocity $|\mathbf{u}|$ is much larger than the ion thermal velocity. Hence the ion mobility can be written as[23]

$$\mu_i \approx \frac{2e\lambda_i}{\pi M|\mathbf{u}|}, \tag{1}$$

where λ_i is the ion-neutral mean free path and e and M are the ion charge and mass. The mobility is large in the center of the discharge where $|\mathbf{u}|$ is small, and is small near the discharge walls where $|\mathbf{u}|$ is large. This variable mobility leads to a nonlinear diffusion

equation to determine the plasma density profile. It is found that the density is relatively uniform within most of the discharge and drops sharply near the discharge walls.

Godyak and Maximov[23,24] have solved the diffusion equations analytically to determine approximate plasma densities at the sheath edges:

$$h_L = \frac{n_{sL}}{n_e} \approx 0.86 \left(3 + \frac{L}{2\lambda_i}\right)^{-1/2} \tag{2}$$

at the axial sheath edge and

$$h_R = \frac{n_{sR}}{n_e} \approx 0.80 \left(4 + \frac{R}{\lambda_i}\right)^{-1/2} \tag{3}$$

at the radial sheath edge. Using these expressions, the electron and ion fluxes leaving the plasma are

$$\Gamma_i = \Gamma_e = n_s u_B \tag{4}$$

for each of the radial and axial sheath edges, where $u_B = (e\mathrm{T}_e/M)^{1/2}$ is the Bohm (ion-sound) velocity and T_e is the electron temperature in units of volts. Therefore the balance of electron-ion pairs generated in the plasma and lost at walls is described as

$$V\frac{dn_e}{dt} = VK_{\mathrm{iz}} n_e n_g - (h_L A_L + h_R A_R) n_e u_B \,, \tag{5}$$

where $V = \pi R^2 L$ is the plasma volume, n_g is the argon density, and $A_L = 2\pi R^2$ and $A_R = 2\pi RL$ are the areas of the axial and radial sheaths. It is assumed that the sheath thickness is negligibly small compared to R and L. The ionization rate constant K_{iz} is obtained from cross section data assuming a Maxwellian velocity distribution of electrons. For argon, $K_{\mathrm{iz}} \approx 2.3 \times 10^{-14} \mathrm{T}_e^{0.68} \exp(-15.76/\mathrm{T}_e)$ m^3/s.

The rate of collisional energy loss within the discharge can be expressed as

$$P_c = en_e n_g V \sum K_i \mathcal{E}_i = en_e n_g V (K_{\mathrm{iz}}\mathcal{E}_{\mathrm{iz}} + K_{\mathrm{ex}}\mathcal{E}_{\mathrm{ex}} + K_{\mathrm{el}}\mathcal{E}_{\mathrm{el}}) \,, \tag{6}$$

where K_{iz}, K_{ex} and K_{el} are the rate constants(m^3/s), and $\mathcal{E}_{\mathrm{iz}}$, $\mathcal{E}_{\mathrm{ex}}$ and $\mathcal{E}_{\mathrm{el}}$ (in volts) are the energies lost per ionization, excitation, and elastic collision, respectively. A part of

the input power is also lost as kinetic energy loss of particles to the walls. This can be described for ions as[25]

$$P_i = e(V_s + \tfrac{1}{2}\mathrm{T_e})(h_L A_L + h_R A_R) n_e u_B \tag{7}$$

and for electrons as

$$P_e = 2e\mathrm{T_e}(h_L A_L + h_R A_R) n_e u_B \,, \tag{8}$$

where

$$V_s = (\mathrm{T_e}/2)\ln(M/2\pi m) \tag{9}$$

is the sheath voltage drop. Therefore, the entire power balance equation is written as

$$\begin{aligned} P_{\mathrm{abs}}(t) =& V\left[\frac{d}{dt}\left(\tfrac{3}{2}en_e\mathrm{T_e}\right) + en_e n_g \sum K_i \mathcal{E}_i\right] \\ &+ e(V_s + \tfrac{5}{2}\mathrm{T_e})(h_L A_L + h_R A_R) n_e u_B \,, \end{aligned} \tag{10}$$

where P_{abs} is the total power absorbed, which is assumed to be known. By solving ordinary differential equations (5) and (10) simultaneously, we obtain $n_e(t)$ and $\mathrm{T_e}(t)$.

In the steady state, $(d/dt \equiv 0)$, (5) and (10) reduce to

$$V K_{\mathrm{iz}} n_e n_g = (h_L A_L + h_R A_R) n_e u_B \tag{11}$$

and

$$P_{\mathrm{abs}} = en_e n_g V \sum K_i \mathcal{E}_i + e(V_s + \tfrac{5}{2}\mathrm{T_e})(h_L A_L + h_R A_R) n_e u_B \,. \tag{12}$$

The plasma density cancels in (11), such that (11) becomes

$$\frac{K_{\mathrm{iz}}(\mathrm{T_e})}{u_B(\mathrm{T_e})} = \frac{h_L A_L + h_R A_R}{n_g V} = \frac{1}{n_g l_{\mathrm{eff}}} \,. \tag{13}$$

The last equality in (13) defines an effective discharge size l_{eff}. Equation (13) determines $\mathrm{T_e}$ for a given gas pressure and discharge geometry (R and L). It is convenient to define a collisional energy loss per electron-ion pair created, $\mathcal{E}_c$, by

$$K_{\mathrm{iz}} \mathcal{E}_c = \sum K_i \mathcal{E}_i \,. \tag{14}$$

$\mathcal{E}_c$ is a function of T_e only, depending on the electron-neutral collisional energy loss processes in the gas[26], and is shown in Fig. 1 for a few pure gases. Then substituting (14) and (11) into (12), we obtain

$$P_{\rm abs} = e\mathcal{E}_T(h_L A_L + h_R A_R) n_e u_B \,, \tag{15}$$

where $\mathcal{E}_T = \mathcal{E}_c + V_s + \frac{5}{2}T_e$ is the total energy loss per electron-ion pair created. Because T_e is known, (15) determines n_e for a given $P_{\rm abs}$. We denote the steady state (cw) solution with a subscript "0".

For typical discharge parameters $p = 5$ mTorr (600 K gas temperature), $P_{\rm abs} = 500$ W, $R = 15.25$ cm, and $L = 7.5$ cm, we obtain $l_{\rm eff} \approx 8.5$ cm, and (13) yields $T_{e0} \approx 3.2$ V and (15) yields $n_{e0} \approx 2.5 \times 10^{11}$ cm^{-3}. For these parameters, $\mathcal{E}_c \approx 30$ V and $\mathcal{E}_T \approx 52$ V. The inclusion of Ar 4s and 4p excited states leads to a 28% reduction in density, with a total of 16% of the ionization taking place from the excited states.[15]

B. Pulsed Power Model

Now, we will discuss the results obtained from a complete argon model (with excited states) assuming that the power is modulated by an ideal rectangular waveform i.e.,

$$\begin{aligned} P_{\rm abs} &= P_{\rm max}, \qquad 0 \le t < \alpha\tau, \\ &= 0, \qquad\quad \alpha\tau \le t < \tau, \end{aligned}$$

in (10), where α is the duty ratio and τ is the period[15]. The time average power was fixed at 500 W. Figures 2(a)–2(c) show the time evolution of the plasma density n_e, the excited atom densities and the electron temperature T_e for three different time periods τ for $P_{\rm abs}(t)$. Each of these graphs shows one cycle of the power on-off duration. During the on-time, 2000 W power is applied and during the off-time the power is 0 W; the duty ratio is 25%. Results representing the 500 W continuous wave (cw) case are also shown in Fig. 2.

For a very short modulation period much less than 10 μs, the electron temperature responds weakly to the modulated power, while the plasma density hardly changes. Therefore both the electron density and the electron temperature are very close to those for the continuous 500 W case. For periods of 10 μs or greater, both the electron temperature and

the plasma density respond to the applied modulated power. For all cases, the electron temperatures first rise sharply to peak values larger than those for the cw case, while the densities hardly change. After this, the temperatures fall and the densities rise, approaching steady values during the pulse on-times. After the pulse is turned off, the temperatures and densities decay toward zero; the temperature decays at a considerably faster rate than the density.

These transient behaviors can be understood from the particle and energy balance equations (5) and (10). Equation (5) can be written as

$$\frac{1}{n_e}\frac{dn_e}{dt} = \nu_{\rm iz} - \nu_{\rm loss}\,, \tag{16}$$

where $\nu_{\rm iz} = K_{\rm iz} n_g$ is the ionization rate and $\nu_{\rm loss} = u_B/l_{\rm eff}$ is a characteristic particle loss rate: $\nu_{\rm iz}$ depends strongly (exponentially) on T_e, and $\nu_{\rm loss}$ depends only weakly on T_e ($\nu_{\rm loss} \propto T_e^{1/2}$). Using (5) to eliminate dn_e/dt in (10) yields

$$\frac{1}{T_e}\frac{dT_e}{dt} = \frac{P_{\rm abs}}{W_e} - \left(\frac{2}{3}\frac{\mathcal{E}_c}{T_e} + 1\right)\nu_{\rm iz} - \left(\frac{2}{3}\frac{V_s + \frac{5}{2}T_e}{T_e} - 1\right)\nu_{\rm loss}\,. \tag{17}$$

where $W_e = \frac{3}{2} e n_e T_e V$ is the plasma energy.

Consider first times just after the pulse turns on. Then as T_e builds up, the last terms on the right hand sides (rhs) of (16) and (17) are small:

$$\frac{1}{n_e}\frac{dn_e}{dt} \approx \nu_{\rm iz}\,, \tag{18}$$

$$\frac{1}{T_e}\frac{dT_e}{dt} \approx \frac{P_{\rm max}}{W_e} - \left(\frac{2}{3}\frac{\mathcal{E}_c}{T_e} + 1\right)\nu_{\rm iz}\,. \tag{19}$$

Initially, T_e is low and the second term on the rhs of (19) is small ($K_{\rm iz}$ is small), leading to a very sharp rise in T_e at a rate $P_{\rm max}/W_e$, up to some maximum value $T_{e\rm max}$. We can estimate $T_{e\rm max}$ by setting $dT_e/dt = 0$ in (19) with $\mathcal{E}_c/T_e \sim 10 \gg 1$ to obtain

$$K_{\rm iz}(T_e) \approx \frac{P_{\rm max}}{n_e n_g e \mathcal{E}_c V}\,. \tag{20}$$

Using the initial density $n_e = n_{e\rm min}$, (20) yields $T_e = T_{e\rm max}$. Beyond this time, (19) remains in quasi-steady state with $d/dt \approx 0$, and T_e falls to its equilibrium value $T_{e\infty}$

($\equiv T_{e0}$ for argon) as n_e increases. If we assume a constant value $\nu_\infty = u_{B\infty}/l_{\rm eff}$ for $\nu_{\rm loss}$, where $u_{B\infty} = (eT_{e\infty}/M)^{1/2}$, then substituting (20) into (16), we obtain

$$\frac{dn_e}{dt} \approx (n_{e\infty} - n_e)\nu_\infty\,, \tag{21}$$

where

$$n_{e\infty} = \frac{P_{\rm max}}{e\mathcal{E}_T V \nu_\infty}\,. \tag{22}$$

We use $\mathcal{E}_T$ rather than $\mathcal{E}_c$ in (22) for consistency with (15) and because we approximate $T_e \approx T_{e\infty}$ during the evolution of n_e to $n_{e\infty}$. The solution to (21) is

$$n_e(t) \approx n_{e\min} + (n_{e\infty} - n_{e\min})\,e^{-\nu_\infty t}, \qquad 0 < \alpha\tau < \tau. \tag{23}$$

For $T_{e\infty} = 3.2$ V, we obtain $\nu_\infty \approx 3.3\times10^4$ s^{-1}, in reasonable agreement with the evolution of n_e seen in Fig. 2(c). Substituting (23) into (20) yields $T_e(t)$.

Consider now times just after the pulse is turned off. Then T_e falls and $\nu_{iz} \ll \nu_{\rm loss}$ in (16) and (17), yielding

$$\frac{1}{n_e}\frac{dn_e}{dt} \approx -\nu_{\rm loss}(t)\,. \tag{24}$$

and

$$\frac{1}{T_e}\frac{dT_e}{dt} \approx -\left(\frac{2}{3}\frac{V_s + \frac{5}{2}T_e}{T_e} - 1\right)\nu_{\rm loss}(t)\,. \tag{25}$$

Using (9), we see that the term in parentheses in (25) has the numerical value of $3.8 \approx 4$ for argon. We see that both T_e and n_e decay with time, but that the decay rate for T_e is faster than the decay rate of n_e by a factor of approximately 4. Using $\nu_{\rm loss}(t) = u_B(T_e)/l_{\rm eff} \propto T_e^{1/2}$, we can solve (25) to obtain the temperature decay

$$T_e(t) = T_{e\infty}[1 + 2\nu_\infty(t - \alpha\tau)]^{-2}\,, \qquad \alpha\tau < t < \tau. \tag{26}$$

A similar result was obtained by Sugai et al[9]. The density decay follows immediately by eliminating ν_∞ from (24) and (25):

$$n_e(t) \approx n_{e\max}[1 + 2\nu_\infty(t - \alpha\tau)]^{-1/2}\,, \qquad \alpha\tau < t < \tau. \tag{27}$$

The decay times from the model of 16 μs and 61 μs for T_e and n_e are in good agreement with the decay times of 10 μs and 50 μs, respectively, seen in Fig. 2(c).

In the preceding analysis we have assumed that the ion losses to the walls are in quasi-equilibrium with the plasma potential V_s whose gradient drives the losses, and hence that $\nu_\infty(t) \propto T_e^{1/2}$. There is some evidence from PIC simulations that this may not be true in the early phase of the decay[16]. Because of their high inertia, ions can initially retain their velocities after the discharge is turned off; hence $\nu_\infty(t) \approx$ const, leading to an initial exponential decay of n_e and T_e found from (24) and (25). However, ions lose their initial velocity within an ion mean free path λ_i, which we assume to be small compared to the discharge size l_{eff}. Therefore, (26) and (27) reasonably represent the overall decay dynamics.

Figure 3 shows cylindrical Langmuir probe measurements of (a) $n_e = n_{\text{Ar}^+}$ and (b) T_e taken in a pulsed ICP discharge driven by a planar rf inductive coil with $p = 5$ mTorr, average power $P_{\text{abs}} = 51$ W, $L = 7.5$ cm, and $R = 15$ cm.[14] The orbital motion limit (OML) theory was used to determine n_{Ar^+} from the ion saturation part of the probe characteristic, and T_e was determined from the transition part of the characteristic. The measured density and temperature (solid lines) are compared in the figure to global model calculations of relative density and absolute temperature (dashed lines). The transient behavior seen experimentally is described well by (23) and (27) for n_e and by (20) and (26) for T_e.

It is noteworthy that, for the same time-average power, the average plasma density for pulsed operation is higher than the density for cw operation. In fact, in Figs. 2(a) and 2(b), the time-varying densities are higher than the cw density for *all* times. Figure 4 shows the relation between the time-average plasma density and the period, with the duty ratio as a parameter. The power applied during the on-time is varied according to the duty ratio so that the time-average power is fixed at 500 W. For a very short period, the plasma densities are very close to that for a continuous power of 500 W. All the curves have peaks at approximately 100 μs, and the peak value increases as the duty ratio decreases. This period is of the order of the fall (loss) time for the plasma density. At a duty ratio of 10%, the maximum plasma density is nearly four times that for 500 W of continuous rf power.

A curve for results obtained at 25% duty ratio using the simpler model which does not include excited state Ar atoms is superimposed. The curve not only shows qualitatively the same trend, but also is quantitatively close to the values which are calculated by the more complete model. The time-average plasma density has been measured as a function of the pulse period over the range of τ's from 10 to 10^4 μs and for duty ratios of 30%, 50%, and 70%.[14] The measurements are in reasonable agreement with the results shown in Fig. 4.

To understand these results from the global model, we equate $n_e(t)$ in (23) to n_{emax} at $t = \alpha\tau$, and $n_e(t)$ in (27) to n_{emin} at $t = \tau$. Solving the resulting two equations, we obtain

$$n_{emin} = n_{e\infty}\frac{e^{\nu_\infty \alpha\tau} - 1}{[1 + 2\nu_\infty(1-\alpha)\tau]^{1/2}e^{\nu_\infty\alpha\tau} - 1}, \tag{28}$$

$$n_{emax} = n_{emin}[1 + 2\nu_\infty(1-\alpha)\tau]^{1/2}. \tag{29}$$

Then time-averaging $n_e(t)$ given by (23) and (27) and using (28) and (29) to eliminate n_{emin} and n_{emax}, we obtain

$$\frac{\langle n_e\rangle}{n_{e0}} = 1 + \frac{1}{\nu_\infty\alpha\tau}\frac{\left[\left(1 + 2\nu_\infty(1-\alpha)\tau\right)^{1/2} - 1\right]^2\left[1 - e^{-\nu_\infty\alpha\tau}\right]}{\left[1 + 2\nu_\infty(1-\alpha)\tau\right]^{1/2} - e^{-\nu_\infty\alpha\tau}}, \tag{30}$$

where $n_{e0} = \alpha n_{e\infty}$ is the density for the cw case having the same average power and gas density as the pulsed case. From (30) we see that $\langle n_e\rangle \to n_{e0}$ for $\nu_\infty\tau \ll 1$ and for $\nu_\infty\tau \gg 1$. Furthermore, $\langle n_e\rangle$ has a maximum for $\nu_\infty\alpha\tau \sim 1$. Considering the case of small α, then (30) yields $\langle n_e\rangle - n_{e0} \approx 0.9n_{e0}/\sqrt{\alpha}$ at $\nu_\infty\alpha\tau \approx 1.3$. These features and scalings can be seen in Fig. 4.

Physically, average densities are higher than peak densities because the electron temperature decreases immediately after the power is turned off. This leads to a decrease of the loss rate of charged particles because the Bohm velocity, which accounts for the particle loss process, is proportional to the square root of the electron temperature. It is found that the product of the average density and average temperature is roughly a constant, varying by no more than 30% over the range of parameters shown in Fig. 4. If the period is very long, as in Fig. 1(c), both the electron temperature and the plasma density are in

quasi-equilibrium with the input power waveform. Consequently, the average T_e and n_e approach the product of the duty ratio times T_e and n_e for the cw case with power P_{max}.

Because T_e drops to low values in the afterglow, the ion acceleration voltage V_s given in (9) will be low there. Figure 5 shows the energy distribution of O_2^+ ions escaping radially to the walls, measured by Charles and Boswell[6] in an rf-driven helicon oxygen discharge that is square wave modulated at 5 kHz, with $p = 2$ mTorr and $P_{in}(on) = 800$ W. Only the middle peak is present for a cw discharge, corresponding to a space charge potential given approximately by (9). The low energy peak represents collection of ions during the afterglow when T_e is low and corresponds to a plasma potential with respect to earth (not the insulated chamber wall) of 10–20 V. The high energy peak is ascribed to a capacitively coupled discharge initiation phase having a high plasma potential at the beginning of the on-time. when the density is low. It is clear that pulsing the discharge can drastically modify the average ion and electron energy distributions. This can have a strong effect on processing issues such as charge build-up damage, notching, etc, as has been observed[3–5].

One should note that the decay of T_e during the off-time when $P_{abs} \equiv 0$ is a singular case. If there is a small but non-zero power absorbed during the off-time,[15] and if the off-time is much greater than the ion loss time, then T_e decays from its initial value toward zero at the beginning of the off-time, but then reaches a minimum value and increases back to its initial value during the remaining part of the off-time. This is a consequence of the steady state particle balance equation (11), which shows that T_e is independent of n_e (and thus P_{abs}) for any non-zero n_e.

Reactions that have threshold energies, e.g., ionization, excitation and chemical reactions, generally have rate constants that are approximately proportional to $\exp(-\mathcal{E}_a/T_e)$. Figure 6 shows time-average characteristic rates $\langle r_a \rangle = \langle n_e \exp(-\mathcal{E}_c/T_e) \rangle$ for such collisional processes having various activation energies $\mathcal{E}_a$. The curves are drawn after normalization by the corresponding values for 500 W cw power application; i.e., $\langle r_a \rangle / r_{a0}$ is shown. The higher activation energies represent reactions such as ionization and electronic excitation. The lower $\mathcal{E}_a$ represents processes such as attachment and dissociation in molecular gases. According to this result, selective control of excitation processes having different activation energies can be achieved by varying the pulse period.

We can understand these results analytically in terms of three limiting regimes of $\mathcal{E}_a$. For $\mathcal{E}_a \lesssim T_{emin}$, where T_{emin} is a characteristic temperature in the afterglow, the reaction rate follows the density variation: $\langle r_a \rangle / r_{a0} = \langle n_e \rangle / n_{e0}$. This leads to a peak in $\langle r_a \rangle / r_{a0}$ for $\nu_\infty \tau \sim 1$, as shown in Fig. 4. For $T_{emin} \lesssim \mathcal{E}_a \lesssim \mathcal{E}_{iz}$, there is a low reaction rate in the afterglow. Hence only the average electron density during the on-time contributes to $\langle r_a \rangle$. Integrating (23) to determine this average and using (28), we find

$$\frac{\langle r_a \rangle}{r_{a0}} = 1 - \frac{1}{\nu_\infty \alpha \tau} \frac{\left[\left(1 + 2\nu_\infty(1-\alpha)\tau\right)^{1/2} - 1\right]\left[1 - e^{-\nu_\infty \alpha \tau}\right]}{\left[1 + 2\nu_\infty(1-\alpha)\tau\right]^{1/2} - e^{-\nu_\infty \alpha \tau}}, \tag{31}$$

which displays a dip in $\langle r_a \rangle / r_{a0}$ near $\nu_\infty \tau \sim 1$, as shown in Fig. 6. For $\mathcal{E}_a \gtrsim \mathcal{E}_{iz}$, the sharp rise in T_e to T_{emax} at the very beginning of the on-time leads to an exponential increase in the reaction rate, yielding a peak in $\langle r_a \rangle / r_{a0}$, as shown in Fig. 6.

III. ELECTRONEGATIVE DISCHARGES

A. Steady State Model

The use of an electronegative molecular gas greatly complicates the analysis of particle and energy balance in high density, low pressure discharges.[22,27] Even for cw power, the high fractional dissociation of the molecular gas implies that neutral particle balance equations for the dissociation fragments are important. These in turn may depend on poorly known rate constants at the chamber walls for recombination, reaction, etc. Furthermore, there can be multiple positive and negative ions, such that the usual assumption of ambipolar diffusion for the charged particle fluxes may not be valid. Also, it is well known that the discharge can stratify into an electronegative core region, surrounded by an electropositive halo region.[27,28] Hence the assumption of relatively uniform particle density profiles in volume-averaged models may not be valid. Some reasonable estimates are required for the profiles of positive ions, negative ions, electrons, and neutrals, obtained from the appropriate diffusion equations. A reasonably complete steady-state volume-averaged model incorporating this information has been given for the diatomic gases O_2 and Cl_2 and for O_2/Ar mixtures.[22]

It is a simplifying feature of typical high density, low pressure, cw processing discharges that the ratio n_-/n_e of negative ion to electron density is often considerably less than unity, even with highly electronegative feedstocks such as Cl_2. Hence, for most practical purposes, the major issue is not the negative ion dynamics, but the dissociation of the gas into multiple neutral and positive ion species. This will also more-or-less be the situation during the on-time of a pulsed discharge. However, for low pulsing frequencies the situation can change markedly when the power is turned off. During the off-time, T_e rapidly decreases and n_e and the positive ion density also decrease due to diffusive losses to the walls. Because negative ions are confined within the discharge by the positive space charge potential there, they are not lost, and, in fact, their density can initially increase. At some point in time, when T_e has dropped to a low enough value, then the potential becomes very small and a diffusive flux of negative ions to the wall is established. This flux can have a profound effect on materials processing at surfaces.

Let us examine the simplest description of the steady state in a high density, low pressure chlorine discharge assuming first that the Cl^- (and Cl_2^-) density is small. Then the particle balance equations for Cl, Cl^+, and Cl_2^+ are

$$2K_{\rm diss} n_e n_{Cl_2} = \nu_{Cl} n_{Cl}, \tag{32}$$

$$K_{\rm iz,Cl}\, n_e n_{Cl} = \nu_{\rm loss,Cl+}\, n_{Cl+}, \tag{33}$$

$$K_{\rm iz,Cl_2}\, n_e n_{Cl_2} = \nu_{\rm loss,Cl_2^+}\, n_{Cl_2^+}, \tag{34}$$

where $K_{\rm diss} \approx 3.8 \times 10^{-8} \exp(-3.825/T_e)$ cm^3/s is the rate constant for electron impact dissociation of Cl_2, $K_{\rm iz,Cl}$ and $K_{\rm iz,Cl_2}$ are the ionization rate constants for production of Cl^+ from Cl and Cl_2^+ from Cl_2, and ν_{Cl}, $\nu_{\rm loss,Cl+}$, and $\nu_{\rm loss,Cl_2^+}$ are the loss rates of Cl, Cl^+, and Cl_2^+ to the vacuum pump and to the walls. In (32), we have assumed that the ionization loss of Cl to produce Cl^+ is nearly balanced by recombination of Cl^+ on the wall, which is recycled back into the discharge. We can estimate

$$\nu_{Cl} \approx \frac{S_p}{V} + \frac{A_L + A_R}{2V} \bar{v}_{Cl} \gamma_{\rm rec}, \tag{35}$$

where S_p is the pumping speed, $\bar{v}_{Cl} = (8eT_g/\pi M)^{1/2}$ is the mean thermal speed of Cl atoms, and γ_{rec} is the recombination coefficient of Cl atoms on the wall. Equation (35) is written in the low pressure limit assuming that gas-phase diffusion is not the rate limiting step for loss of chlorine atoms to the wall. Gas-phase diffusion must be included at higher pressures, $\lambda_{Cl} \lesssim \gamma\Lambda_{Cl}/4$, where λ_{Cl} is the chlorine atom mean free path and Λ_{Cl} is the effective diffusion length[22]. Along with the quasi-neutrality condition,

$$n_e = n_{Cl+} + n_{Cl_2^+}, \tag{36}$$

the energy balance relation

$$P_{abs} = Ve(\mathcal{E}_{T,Cl}\,\nu_{loss,Cl+}\,n_{Cl+} + \mathcal{E}_{T,Cl_2}\,\nu_{loss,Cl_2^+}\,n_{Cl_2^+}), \tag{37}$$

and specification of the neutral density (discharge pressure).

$$n_g = n_{Cl} + n_{Cl_2}. \tag{38}$$

(32)-(34) and (36)-(38) can be solved to determine n_{Cl}, n_{Cl_2}, n_{Cl+}, $n_{Cl_2^+}$, n_e, and T_e for a given n_g and P_{abs}. The full analytic solution is messy and not particularly illuminating. However, we can simplify further by considering that the corresponding rate constants for the atomic and molecular species are approximately equal. This is not a bad assumption in chlorine discharges at low pressures. Then adding (33) and (34) and using (38), we obtain

$$K_{iz}(T_e)n_g \approx \nu_\infty(T_e), \tag{39}$$

which determines T_e [compare to (13)]. Using (36) in (37), we obtain n_e [compare to (15)]:

$$n_e \approx \frac{P_{abs}}{Ve\mathcal{E}_T\nu_\infty}. \tag{40}$$

Using (36), (38), and (39) in (32) we determine the dissociation ratio

$$\frac{n_{Cl}}{n_{Cl_2}} \approx \frac{2K_{diss}n_e}{\nu_{Cl}}, \tag{41}$$

and the ratio of (33) to (34) yields

$$\frac{n_{Cl+}}{n_{Cl_2^+}} \approx \frac{n_{Cl}}{n_{Cl_2}}. \tag{42}$$

Eliminating n_{Cl_2} in (41) using (38), we obtain the cw chlorine atom density:

$$n_{Cl0} = n_g \frac{2K_{diss} n_{e0}}{2K_{diss} n_{e0} + \nu_{Cl}}. \tag{43}$$

For $\gamma \approx 0.05$, typical for chlorine on reactor walls, and for $T_e \approx 3$ V, then $\nu_{Cl} \approx 600\ s^{-1}$, $\nu_\infty \approx 3 \times 10^4\ s^{-1}$, and $K_{diss} \approx 1 \times 10^{-8}\ cm^3/s$. At 5 mTorr (600 K), $n_g \approx 8.3 \times 10^{13}\ cm^{-3}$, and taking a typical value of $n_e = 2 \times 10^{11}\ cm^{-3}$, (41) yields $n_{Cl}/n_{Cl_2} \approx 6.6$. Therefore, the discharge is highly dissociated.

Let us, *post hoc*, consider the negative ion particle balance

$$K_{att} n_e n_{Cl_2} = K_{rec}(n_{Cl+} + n_{Cl_2^+}) n_{Cl-}, \tag{44}$$

where $K_{att} \approx 2.4 \times 10^{-10}\ cm^3/s$ is the dissociative attachment rate constant and $K_{rec} \approx 5 \times 10^{-8}\ cm^3/s$ is the rate constant for positive-ion/negative-ion mutual neutralization. Using (36) in (44), we find

$$n_{Cl-} \approx \frac{K_{att} n_{Cl_2}}{K_{rec}}.$$

Using (38), this can be rewritten as

$$n_{Cl-} \approx \frac{K_{att} n_g}{K_{rec}} \left(1 + \frac{n_{Cl}}{n_{Cl_2}}\right)^{-1}. \tag{45}$$

For $n_{Cl}/n_{Cl_2} \approx 6.6$, we find $n_{Cl-} \approx 5.2 \times 10^{10}\ cm^{-3}$. We see that $n_{Cl-}/n_e \approx 0.26$; hence the negative ions are 21% of the total negative charge in the discharge.

Figures 7 and 8 show n_{Cl-}/n_e and the fractional dissociation n_{Cl}/n_g versus γ_{rec} for pressures of 1, 10, and 100 mTorr at an operating power of 1000 W, based on a more complete global chlorine model of Lee and Lieberman.[22] For pressures between 1 and 10 mTorr and for recombination coefficients less than 0.1, the discharge is seen to be highly dissociated, and the ratio of n_{Cl-}/n_e is considerably less than unity, in agreement with the preceding steady state model.

B. Pulsed Power Model

Neutral Radical Dynamics

Now let us examine the neutral radical dynamics for pulsed discharges in the highly dissociated regime. Equation (32) becomes

$$\frac{dn_{\mathrm{Cl}}}{dt} = 2K_{\mathrm{diss}} n_e n_{\mathrm{Cl}_2} - \nu_{\mathrm{Cl}} n_{\mathrm{Cl}}. \tag{46}$$

Because n_{Cl} varies with time, n_{Cl_2} does also. We assume that these variations are fast compared to the pumping rate S_p/V. Hence we write

$$2n_{\mathrm{Cl}_2}(t) + n_{\mathrm{Cl}}(t) = n_a = \text{ const}, \tag{47}$$

where n_a is the total density of chlorine atoms in both atomic and molecular form. The gas density given by (38) then varies with time, having an average value

$$\langle n_g \rangle = \tfrac{1}{2}(n_a + \langle n_{\mathrm{Cl}} \rangle). \tag{48}$$

However, we retain a constant λ_i in (2) and (3) for ease of analysis. When comparing pulsed and cw discharges, we should choose $\langle n_g \rangle$ for the pulsed discharge equal to n_g for the cw discharge.

Eliminating n_{Cl_2} from (46) using (47), we obtain the differential equation

$$\frac{dn_{\mathrm{Cl}}}{dt} + \nu_{\mathrm{rise}}(t) n_{\mathrm{Cl}} = K_{\mathrm{diss}}(\mathrm{T}_e(t)) n_e(t) n_a \,, \tag{49}$$

where

$$\nu_{\mathrm{rise}}(t) = K_{\mathrm{diss}}(\mathrm{T}_e(t)) n_e(t) + \nu_{\mathrm{Cl}} \,. \tag{50}$$

From (49) and (50), we see that the characteristic build-up rate for the Cl atom density is $\nu_{\mathrm{rise}} = K_{\mathrm{diss}} n_e + \nu_{\mathrm{Cl}}$, and the characteristic decay rate is ν_{Cl}. For our parameters, which are typical, $\nu_{\mathrm{rise}} \approx 2600\ \mathrm{s}^{-1}$ and $\nu_{\mathrm{Cl}} \approx 600\ \mathrm{s}^{-1}$. These rates are both slow compared to characteristic electron density and temperature build-up and decay rates. Therefore, (49) reduces to two cases that are not mutually exclusive for pulsed discharges. For the first case with $\nu_{\mathrm{rise}}\tau \ll 1$, we have that $n_{\mathrm{Cl}}(t) \approx \text{ const } \equiv \langle n_{\mathrm{Cl}} \rangle$. Then (49) reduces to (32) with a time-varying production rate $K_{\mathrm{diss}} n_e$. Assuming a dissociation energy such that

$T_{emin} \lesssim \mathcal{E}_{diss} \lesssim \mathcal{E}_{iz}$ and averaging (32) over time, we obtain $\langle n_{Cl}\rangle/n_{Cl0} = \langle r_a\rangle/r_{a0}$ as given in (31), with n_{Cl0} given by (43).

For the second case $\nu_{\infty}\tau \gg 1$, we can treat $n_e(t)$ and $T_e(t)$ as rectangular waveforms. During the on-time, $n_e(t) = n_{e\infty}$ and $T_e(t) = T_{e\infty}$. The solution of (49) is then

$$n_{Cl}(t) = n_{Cl\infty} - (n_{Cl\infty} - n_{Clmin})e^{-\nu_{rise}t}, \qquad 0 < t < \alpha\tau, \tag{51}$$

where $\nu_{rise} = K_{diss}(T_{e\infty}) + \nu_{Cl}$. During the off-time, n_e and T_e are approximately zero and the solution of (49) is

$$n_{Cl}(t) = n_{Clmax}e^{-\nu_{Cl}(t-\alpha\tau)}, \qquad \alpha\tau < t < \tau. \tag{52}$$

As for the electron density waveform treated previously, we set $n_{Cl}(t) = n_{Clmax}$ at $t = \alpha\tau$ in (51), and $n_{Cl}(t) = n_{Clmin}$ at $t = \tau$ in (52), and simultaneously solve these two equations to obtain

$$n_{Clmin} = n_{Cl\infty}\frac{e^{\nu_{rise}\alpha\tau} - 1}{e^{\nu_{rise}\alpha\tau + \nu_{Cl}(1-\alpha)\tau} - 1}, \tag{53}$$

$$n_{Clmax} = n_{Clmin}e^{\nu_{\infty}(1-\alpha)\tau}. \tag{54}$$

Then integrating (51) and (52) over time and using (53) and (54) to eliminate n_{Clmin} and n_{Clmax}, we find

$$\langle n_{Cl}\rangle = F n_{Cl\infty}, \tag{55}$$

where

$$F = \alpha + \frac{1}{\tau}\left(\frac{1}{\nu_{Cl}} - \frac{1}{\nu_{rise}}\right)\frac{(e^{\nu_{rise}\alpha\tau} - 1)(e^{\nu_{Cl}(1-\alpha)\tau} - 1)}{e^{\nu_{rise}\alpha\tau + \nu_{Cl}(1-\alpha)\tau} - 1}. \tag{56}$$

Substituting (47) into (41) to eliminate n_{Cl_2}, we find

$$n_{Cl\infty} = \left(1 - \frac{\nu_{Cl}}{\nu_{rise}}\right)n_a. \tag{57}$$

Substituting (48) into (57) to eliminate n_a and inserting this into (55), we obtain

$$\langle n_{Cl}\rangle = \frac{2\left(1 - \frac{\nu_{Cl}}{\nu_{rise}}\right)F}{1 + \left(1 - \frac{\nu_{Cl}}{\nu_{rise}}\right)F}\langle n_g\rangle. \tag{58}$$

Dividing (58) by (43) yields $\langle n_{Cl}\rangle/n_{Cl0}$.

Equation (58) has two regimes depending on whether $\nu_{Cl}(1-\alpha)\tau$ is much less than or much greater than unity. In the first regime, $F \to 1$ and we find

$$\langle n_{Cl} \rangle = \frac{2K_{diss} n_{e\infty}}{2K_{diss} n_{e\infty} + \nu_{Cl}} \langle n_g \rangle. \tag{59}$$

Furthermore, $n_{Cl}(t)$ is very weakly modulated; i.e., $n_{Cl}(t) \approx$ const. In this regime, it is remarkable that $\langle n_{Cl} \rangle$ depends only on $n_{e\infty}$, independent of the duty ratio α; i.e., $\langle n_{Cl} \rangle$ depends only on the *peak* power P_{max}, and not on the average power P_{abs}. Therefore, reducing α at fixed P_{max} reduces the average energy flux to the walls (and substrate) without affecting the neutral radical flux, as has been observed experimentally by Charles et al[6]. This can have important surface processing implications. We can estimate the optimum α and τ to minimize the energy flux while maintaining the radical flux by setting $\nu_{rise}\alpha\tau \sim 1$ and $\nu_{Cl}(1-\alpha)\tau \sim 1$ (an on-time of order ν_{rise}^{-1} and and off-time of order ν_{Cl}^{-1}). For our example we obtain $\tau \sim 250$ μs and $\alpha \sim (\nu_{rise}/\nu_{Cl} + 1)^{-1} \approx 13\%$, such that the time average power is 13% of the cw power for roughly the same radical generation.

In the second regime where $\nu_{Cl}(1-\alpha)\tau \gg 1$, then the variation of $n_{Cl}(t)$ follows the variation of $n_e(t)$, and $F \to \alpha$. From (58) we obtain

$$\langle n_{Cl} \rangle = \frac{2K_{diss} n_{e0}}{K_{diss} n_{e0}(1+\alpha^{-1}) + \nu_{Cl}} \langle n_g \rangle. \tag{60}$$

Hence $\langle n_{Cl} \rangle$ depends both on the average electron density and on α. The maximum $\langle n_{Cl} \rangle$ occurs at high n_{e0} (high average power) and decreases as α decreases:

$$\langle n_{Cl} \rangle = \frac{2\alpha}{1+\alpha} \langle n_g \rangle. \tag{61}$$

Table 1 gives a summary of the variations of $n_e(t)$ and $n_{Cl}(t)$ in various regimes of the period τ.

The transition between the $\nu_{Cl}(1-\alpha)\tau \ll 1$ and $\nu_{Cl}(1-\alpha)\tau \gg 1$ regimes was studied experimentally by Herrick et al[29] for F atom etching of silicon in an SF_6 pulsed helicon discharge with $\alpha = 1/3$. They measured the relative F atom concentration $n_F(t)$ and the etch rate, which they showed was proportional to $\langle n_F \rangle$. Their results for $n_F(t)$ are in

reasonable agreement with the variations (51) and (52) with $\nu_F \sim 100\ s^{-1}$, and the etch rate varied with τ in a manner described by (55) and (56).

For very long off-times, the discharge can extinguish or can enter a different operating mode during the initial phase of the on-time; e.g., a capacitively coupled mode for an inductive or helicon discharge, or a "low mode"[30] for an electron cyclotron discharge. In such cases new physical phenomena can arise, such as weak power absorption[30] or multipacting[31], that are not described by the global model and are beyond its scope.

Negative Ion Dynamics During Off-Time

We now take $t = 0$ to be the time when the pulse is turned off and examine the negative ion dynamics. Again considering a highly dissociated discharge with an initial negative ion density that is small compared to the electron density, the initial phase of the positive ion density decay is, from (27),

$$\frac{n_{Cl+}(t)}{n_{Cl+}(0)} = \frac{1}{(1+2\nu_\infty t)^{1/2}}. \tag{62}$$

The evolution of the negative ion density is described by

$$\frac{dn_{Cl-}}{dt} = K_{att} n_e(t) n_{Cl_2}(0) - K_{rec} n_{Cl+}(t) n_{Cl-}(t). \tag{63}$$

where $n_{Cl_2}(0)$ is the chlorine molecule density at the beginning of the off-time. Assuming a fixed value for K_{att}, and using quasineutrality ($n_e = n_{Cl+} - n_{Cl-}$) and (62), we obtain

$$\frac{dn_{Cl-}}{dt} + P n_{Cl-} = Q, \tag{64}$$

where

$$P = \nu_{att} + \frac{\nu_{rec}}{(1+2\nu_\infty t)^{1/2}}, \tag{65a}$$

$$Q = n_{Cl+}(0)\,\frac{\nu_{att}}{(1+2\nu_\infty t)^{1/2}}, \tag{65b}$$

with $\nu_{att} = K_{att} n_{Cl_2}(0)$ and $\nu_{rec} = K_{rec} n_{Cl+}(0)$. The solution to (64) is

$$n_{Cl-}(t) = n_{Cl+}(0)\, e^{-s(t)} \int_0^t e^{s(t')} \frac{\nu_{att} dt'}{(1+2\nu_\infty t')^{1/2}} + n_{Cl-}(0)\, e^{-s(t)}, \tag{66}$$

where

$$s(t) = \nu_{att} t + \frac{\nu_{rec}}{\nu_\infty}[(1 + 2\nu_\infty t)^{1/2} - 1]. \tag{67}$$

The integral in (66) can be performed by introducing a change of variables from t to $y = (\nu_{rec}/\nu_\infty)[(1 + 2\nu_\infty t)^{1/2} - 1]$. The result is

$$\begin{aligned}\frac{n_{Cl^-}(t)}{n_{Cl^+}(0)} = &\sqrt{\frac{2\nu_{att}}{\nu_\infty}} \exp\left(-\frac{\nu_{rec}^2}{2\nu_\infty n u_{att}} - \frac{\nu_{att}}{2\nu_\infty} - \frac{\nu_{rec}}{\nu_\infty}(1 + 2\nu_\infty t)^{1/2} - \nu_{att} t\right) \\ &\times \left[G\left(\frac{\nu_{rec}}{\sqrt{2\nu_\infty \nu_{att}}} + \frac{\nu_{att}}{\sqrt{2\nu_\infty \nu_{att}}}(1 + 2\nu_\infty t)^{1/2}\right) - G\left(\frac{\nu_{rec} + \nu_{att}}{\sqrt{2\nu_\infty \nu_{att}}}\right)\right] \\ &+ \frac{n_{Cl^-}(0)}{n_{Cl^+}(0)} \exp\left(\frac{\nu_{rec}}{\nu_\infty} - \frac{\nu_{rec}}{\nu_\infty}(1 + 2\nu_\infty t)^{1/2} - \nu_{att} t\right), \end{aligned} \tag{68}$$

where

$$G(\zeta) = \int_0^\zeta e^{\zeta'^2} d\zeta' = \frac{\sqrt{\pi}}{2i} \operatorname{erf}(i\zeta). \tag{69}$$

The initial value of n_{Cl^-} is

$$\frac{n_{Cl^-}(0)}{n_{Cl^+}(0)} = \frac{\nu_{att0}}{\nu_{att0} + \nu_{rec}}. \tag{70}$$

where ν_{att0} is the attachment rate at $T_e \approx 3$ V. After the power is turned off, T_e decreases and ν_{att} increases for chlorine. We can take ν_{att} to be larger than ν_{att0} in (68) to represent this effect. For our standard case ($p = 5$ mTorr, $n_e = 2 \times 10^{11}$ cm^{-3}), we estimate $\nu_\infty \approx 2.4 \times 10^4$ s^{-1}, $\nu_{rec} \approx 10^4$ s^{-1}, and $\nu_{att0} \approx 2.7 \times 10^3$ s^{-1}. Then from (70), we find $n_{Cl^-}(0)/n_{Cl^+}(0) \approx 0.21$. The results are shown in Fig. 9. For $\nu_{att} = \nu_{att0}$, the solution (68) for n_{Cl^-} is constant at first and then slowly decays to, ultimately, join the decay (62) of the positive ion density. For $\nu_{att} = 3\nu_{att0}$, n_{Cl^-} increases to a maximum value 36% higher than its initial value at $\nu_\infty t \approx 2$, and then joins the decay of n_{Cl^+}. For $\nu_{att} = 10\nu_{att0}$, n_{Cl^-} increases by more than a factor of two at $\nu_\infty t \approx 1.5$ and joins the decay of n_{Cl^+}.

The preceding description of positive and negative ion dynamics is not correct when n_{Cl^-} increases such that $n_{Cl^-}(t) \gtrsim n_e(t)$. In this more electronegative regime, the positive ion diffusion loss rate changes.[22] Also, positive ions are increasingly lost in the volume by mutual neutralization with negative ions. Furthermore, the decay of T_e saturates at a temperature of order the gas temperature. These dynamics modify the assumed form (62) for the positive ion decay, rendering (68) invalid. In addition, the preceding solution for

n_{Cl^-} fails when T_e drops so low that the space charge potential V_s no longer confines the negative ions. In that case a significant negative ion flux springs up at the walls, and the resulting loss term must be included in (63).

The subsequent decay of this positive-negative ion plasma is not governed by the low pressure diffusion solutions (2) and (3); the characteristic diffusion rate for decay of the fundamental mode is D_{ai}/Λ^2, where Λ is the diffusion length given by

$$\frac{1}{\Lambda^2} = \left(\frac{\pi}{L}\right)^2 + \left(\frac{2.405}{R}\right)^2 , \tag{51}$$

and D_{ai} is the ambipolar diffusion coefficient for positive and negative ions having diffusion coefficients D_{Cl^+} and D_{Cl^-} and mobilities μ_{Cl^+} and μ_{Cl^-}:

$$D_{ai} = \frac{D_{Cl^-}\,\mu_{Cl^+} + D_{Cl^+}\,\mu_{Cl^-}}{\mu_{Cl^+} + \mu_{Cl^-}} . \tag{52}$$

With $\Lambda \approx 2.2$ cm and an estimate $D_{ai} \sim 3 \times 10^4$ cm^2/s, we obtain a loss rate of $\nu_{diff} \sim 6 \times 10^3$ s^{-1}. which is comparable to the recombination rate in the discharge. The recombination losses become less important as the densities continue to decay. Hence, a considerable fraction of the charged particles striking the walls are low energy negative ions. This can have significant implications for materials processing applications, as has been observed by Mieno and Samukawa[5] and by Shindo and Horiike[11]. Furthermore, Samukawa et al[32] have shown that negative ions can be extracted by application of low frequency (600 kHz) rf bias to the substrate holder.

Mieno and Samukawa[5] have measured the decay of the ion and electron saturation currents, J_{is} and J_{es}, after the power is turned off ($t = 0$) in an ECR chlorine discharge with $p = 2$ mTorr, P_{in}(on) = 500 W, $\tau = 200$ μs, and $\alpha = 50\%$. They used a cylindrical Langmuir probe biased to -20 V. They observe an increase of a factor of 10 in J_{is}/J_{es}, 70 μs after the discharge is turned off. During this same time interval, n_e decreases by a factor of 8, and T_e decreases by a factor of 20. Let us note[33] that the ion saturation current collected by a cylindrical probe biased at high negative voltages is $J_{is} \propto n_{Cl^+}$, independent of T_e, whereas the electron saturation current is $J_{es} \propto n_e T_e^{1/2}$. Hence we find

$$\frac{J_{is}}{J_{es}} \propto \frac{n_{Cl^+}}{n_e T_e^{1/2}} .$$

Because T_e has decreased by a factor of 20 and J_{is}/J_{es} has increased by a factor of 10, we find that $n_{Cl^-}/n_e \approx 1.2$ at $t = 70$ μs; i.e., roughly half the negative charge at this time is in the form of negative ions.

The preceding estimate is consistent with recent work by Ahn et al[10] in an rf-inductively excited (ICP) pulsed chlorine discharge ($\tau = 100$ μs, $\alpha = 50\%$). They measured n_e and T_e using a planar Langmuir probe, n_e using an electron-beam excited plasma oscillation detection method, and n_{Cl^-} using a laser photodetachment method. The electrons are detached from the negative ions by an 0.3 μs ultraviolet XeCl excimer laser pulse, and the sudden increase in n_e is measured. Figure 10 shows n_e and T_e in chlorine ($p = 8$ mTorr, P_{in}(on) = 400 W), and, for comparison, in argon ($p = 6$ mTorr, P_{in}(on) = 200 W). We see the characteristic feature in the afterglow that T_e falls more rapidly than n_e for both chlorine and argon. as predicted by (26) and (27) for argon. The decay of n_e for chlorine is faster than the decay for argon for two reasons: (1) T_e falls faster for chlorine, probably due to the higher collisional energy losses in the molecular component of the neutral gas. Figure 1 shows. for example. that $\mathcal{E}_c$ roughly doubles for a $20\%Cl_2/80\%Cl$ mixture at $T_e \approx 1$ V. (2) n_e falls faster than n_{Cl^+} because n_{Cl^-} increases or remains relatively constant during the decay of n_e. The crosses in Fig. 10(a) give n_e after photodetachment (sum of $n_e + n_{Cl^-} = n_{Cl^+}$ before photodetachment) and the solid dots give n_e. By subtraction one obtains the negative ion density variation shown in Fig. 11. These data show that n_{Cl^-} increases from approximately 1×10^{10} cm^{-3} at $t = 0$ to a maximum of approximately 2×10^{10} cm^{-3} at $t = 25$ μs, after which n_{Cl^-} again decreases (falling portion of the dashed curve for $t > 25$ μs). This type of behavior is predicted by (48), as shown in Fig. 9, provided that the attachment rate ν_{att} increases from its initial value to a larger value within the afterglow. This is indeed the case for chlorine; for example, ν_{att} increases by of order a factor of six as T_e varies from 3 to 0.05 V in the afterglow[19]. Similar phenomena have been observed experimentally in pulsed power oxygen discharges[34]. In that case the increase in ν_{att} has been ascribed to electron attachment to a set of metastable ($^3\Sigma_u^+$, $^3\Delta_u$, $^1\Sigma_u^-$) O_2 states.

We conclude that global models of pulsed-power electropositive discharges in atomic (noble) gases can be very useful in describing quantitatively the transient behavior of the

plasma density and electron temperature. In electronegative molecular gases, such models are less well developed. Although they have not been shown to capture all details of the transient behavior of the neutral radicals and negative ions, they provide great insight into the qualitative behavior. However, such issues as stratification of the discharge into an electronegative core and and an electropositive edge region, neutral interactions with the chamber walls, the nature of the diffusive solutions in the electronegative core, and the changes in transport and rate coefficients as the electron temperature decreases to very low values in the afterglow need to be considered further.

The authors gratefully acknowledge helpful discussions with C. Lee. This work was partially supported by NSF Grant ECS-9217500, DOE Grant DE-FG03-87ER13727, LLNL Grant W-7405-ENG-48, and by the Lam Research Corporation. One of the authors (SA) thanks Toshiba Corporation for enabling his visit to U.C. Berkeley.

REFERENCES

1. S. Samukawa and S. Furuoya, *Appl. Phys. Lett.* **63** 2044 (1993).

2. S. Samukawa, *Jpn. J. Appl. Phys. Pt. 1* **33** 2133 (1994).

3. S. Samukaya, *Appl. Phys. Lett.* **64** 3398 (1994).

4. S. Samukawa and K. Terada, *J. Vac. Sci. Technol.* **B12** 3300 (1994).

5. T. Mieno and S. Samukawa, *Jpn. J. Appl. Phys. Pt. 2* **34** 1079 (1995).

6. C. Charles and R.W. Boswell. *J. Appl. Phys.* **78** 766 (1995).

7. C. Charles, R.W. Boswell, and H. Kuwahara, *Appl. Phys. Lett.* **67** 40 (1995).

8. A.E. Wendt, L.J. Mahoney, and J.L. Shohet, *Bull. Am. Phys. Soc.* **XXX** XXX (19XX).

9. H. Sugai, K. Nakamura, Y. Hikosaka, and M. Nakamura, *J. Vac. Sci. Technol.* **A13** 887 (1995).

10. T.H. Ahn, K. Nakamura, and H. Sugai, submitted to *Appl. Phys. Lett.* **XXX** XXX (1995).

11. H. Shindo and Y. Horiike, "Silicon Etching Employing Bipolar Ions in Plasma," Abstract J4, p. 41, Proceedings of the IUVSTA International Workshop on Plasma Sources and Surface Interactions in Plasma Processing, September 20–22, 1995, Fuji-Yoshida, Japan.

12. Ch. Hollenstein, A.A. Howling, L. Sansonnens, J.-L. Dorier and C. Courteille, "Negative Ions and Particulates in Silane Plasmas," Abstract H1, p. 32, Proceedings of the IUVSTA International Workshop on Plasma Sources and Surface Interactions in Plasma Processing, September 20–22, 1995, Fuji-Yoshida, Japan.

13. H. Nogami, Y. Ogahara, K. Mashimo, Y. Nakagawa and T. Tsukada, "SiO_2 Etching by $M = 0$ Helicon Plasma," Abstract D4, p. 17, Proceedings of the IUVSTA International Workshop on Plasma Sources and Surface Interactions in Plasma Processing, September 20–22, 1995, Fuji-Yoshida, Japan.

14. S. Ashida, M.R. Shim, and M.A. Lieberman, submitted to *J. Vac. Sci. Technol.* **AXX** XXX (1995).

15. S. Ashida, C. Lee, and M.A. Lieberman, *J. Vac. Sci. Technol.* **A13** 2498 (1995).

16. R.W. Boswell and D. Vender, *IEEE Trans. Plasma Sci.* **19** 141 (1991).

17. J.D. Bukowski, R.A. Stewart, D.B. Graves, and P. Vitello, *J. Electrochem. Soc.* **XXX** XXX (1995).

18. V. Vahedi, M.A. Lieberman, G. DiPeso, and D.W. Hewett, "2D Modeling of Time Modulated Inductive Discharges," 41st National Symposium, American Vacuum Society, October 24-28, 1994, Denver, CO.

19. S. Ashida and M.A. Lieberman, submitted to *Jpn. J. Appl. Phys.* **XXX** XXX (1995).

20. L.J. Overzet and F.Y. Leong-Rousey, *Plasma Sources Sci. Technol.* 4 432 (1995).

21. C. Lee, D.B.Graves, M.A. Lieberman and D.W. Hess, *J. Electrochem. Soc.* **141** 1546 (1994).

22. C. Lee and M.A. Lieberman, *J. Vac. Sci. Technol.* **A13** 368 (1995).

23. M.A. Lieberman and A.J. Lichtenberg, *Principles of Plasma Discharges and Materials Processing,* (J. Wiley, New York, 1994) Sec. 5.3.

24. See, for example, V.A. Godyak, *Soviet Radio Frequency Discharge Research,* (Delphic Associates, Inc., Falls Church, VA, 1986) Chap. 5.

25. See reference 23, Sec. 10.2.

26. See reference 23, p. 81.

27. See reference 23, Sec. 10.3.

28. A.J. Lichtenberg, V. Vahedi, M.A. Lieberman and T. Rognlien, *J. Appl. Phys.* **75** 2339 (1994); **76** 625 (1994).

29. A. Herrick, A.J. Perry, and R.W. Boswell, "Silicon Etching by SF_6 in a Pulsed Helicon Reactor," Abstract PI-13, p. 56, Proceedings of the IUVSTA International Workshop on Plasma Sources and Surface Interactions in Plasma Processing, September 20–22, 1995, Fuji-Yoshida, Japan.

30. D.A. Carl, M.C. Williamson, M.A. Lieberman, and A.J. Lichtenberg, *J. Vac. Sci. Technol.* **B9** 339 (1991).

31. R.W. Boswell and D. Vender, "An Experimental Study of Breakdown in a Pulsed Helicon Plasma," Abstract PI-12, p. 55, Proceedings of the IUVSTA International Workshop on Plasma Sources and Surface Interactions in Plasma Processing, September 20–22, 1995, Fuji-Yoshida, Japan.

32. S. Samukawa, K. Kinoshita, and T. Mieno, "Pulse-time Modulated Plasma Etching of Etching Processes for Overcoming Limitation,", Abstract B1, p. 5, Proceedings of the IUVSTA International Workshop on Plasma Sources and Surface Interactions in Plasma Processing, September 20–22, 1995, Fuji-Yoshida, Japan.

33. See reference 23, Sec. 6.6.

34. D. Hayashi, K. Ura, K. Susaki, and K. Kadota, "Measurement of Negative Ions in High Density Oxygen Plasma by Probe-Assisted Laser Photodetachment Method," Abstract PII-9, p. 81, Proceedings of the IUVSTA International Workshop on Plasma Sources and Surface Interactions in Plasma Processing, September 20–22, 1995, Fuji-Yoshida, Japan.

FIGURE CAPTIONS

Figure 1. Collisional energy loss $\mathcal{E}_c$ per electron-ion pair created versus T_e; note the differences between molecular and atomic species (from reference 22).

Figure 2. Time evolution of the plasma density n_e, the electron temperature T_e and the excited atom (4s and 4p) densities for different periods τ, for a time-average power of 500 W and a duty ratio of 25%; (a) $\tau = 10$ μs; (b) $\tau = 100$ μs; (c) $\tau = 1$ ms (from reference 15).

Figure 3. Time resolved plasma density and electron temperature; the solid curves show the experimental results: the dashed curves show the global model results; time-average power is 51 W: (a) electron density, period = 100 μs: (b) electron temperature, period = 250 μs (from reference 14).

Figure 4. Plasma densities averaged over one period of the modulated power, with duty ratio as a parameter: the power applied during the on-time was varied so that the time average power is fixed at 500 W for all the calculations; a curve representing the simple model without excited states is also shown (from reference 15).

Figure 5. Ion energy distribution function for O_2^+ ions escaping radially to the walls; 250 μs on, 125 μs off (from reference 6).

Figure 6. Time-average characteristic generation rate of particles which have different activation energies; duty ratio=25%, time-average applied power=500 W (from reference 15).

Figure 7. Ratio n_{Cl^-}/n_e of negative ion to electron density vs wall recombination coefficient γ_{rec} for a chlorine discharge; absorbed power = 1000 W; flow rate = 35 sccm (from reference 22).

Figure 8. Fractional dissociation n_{Cl}/n_g vs wall recombination coefficient γ_{rec} for a chlorine discharge; absorbed power = 1000 W; flow rate = 35 sccm (from reference 22).

Figure 9. Time variation of n_{Cl^+} using equation (62) and of n_{Cl^-} using equation (68) from a global model analysis.

Figure 10. Time variation of (a) electron density n_e and (b) electron temperature T_e for 100 μs period and 50% duty cycle in chlorine (8 mTorr, 400 W) and in argon (6 mTorr, 200 W); the open and closed circles indicate the data for Ar and Cl_2, respectively; the crosses in (a) indicate the data obtained after photodetachment (from reference 10).

Figure 11. Time variation of negative ion density n_{Cl-} and of n_{Cl-}/n_{Cl+} (in percent); the dashed line indicates the relative n_{Cl-} obtained from Langmuir probe measurements, matched to n_{Cl-} at 25 μs; the relative measurements are not valid for $t < 0$ (from reference 10).

τ regime	$\nu_\infty\tau \ll 1$ $\nu_{\rm rise}\alpha\tau \ll 1$ $\nu_{\rm Cl}(1-\alpha)\tau \ll 1$	$\nu_\infty\tau \sim 1$ $\nu_{\rm rise}\alpha\tau \ll 1$ $\nu_{\rm Cl}(1-\alpha)\tau \ll 1$	$\nu_\infty\tau \gg 1$ $\nu_{\rm rise}\alpha\tau \gg 1$ $\nu_{\rm Cl}(1-\alpha)\tau \ll 1$	$\nu_\infty\tau \gg 1$ $\nu_{\rm rise}\alpha\tau \gg 1$ $\nu_{\rm Cl}(1-\alpha)\tau \gg 1$
$n_e(t)$ waveform	const	rise and decay	rectangular	rectangular
$n_{\rm Cl}(t)$ waveform	const	const	const	rectangular
$\langle n_{\rm Cl}\rangle/\langle n_g\rangle$	cw case	depends on $\langle n_e\rangle$	depends on $n_{e\infty}$	depends on n_{e0} and α
$\langle n_{\rm Cl}\rangle/\langle n_g\rangle$ at high power	1	1	1	$2\alpha/(1+\alpha)$

Table 1. Regimes of n_e and $n_{\rm Cl}$ vs τ; the ordering $\nu_\infty \gg \nu_{\rm rise}\alpha \gtrsim \nu_{\rm Cl}(1-\alpha)$ is assumed.

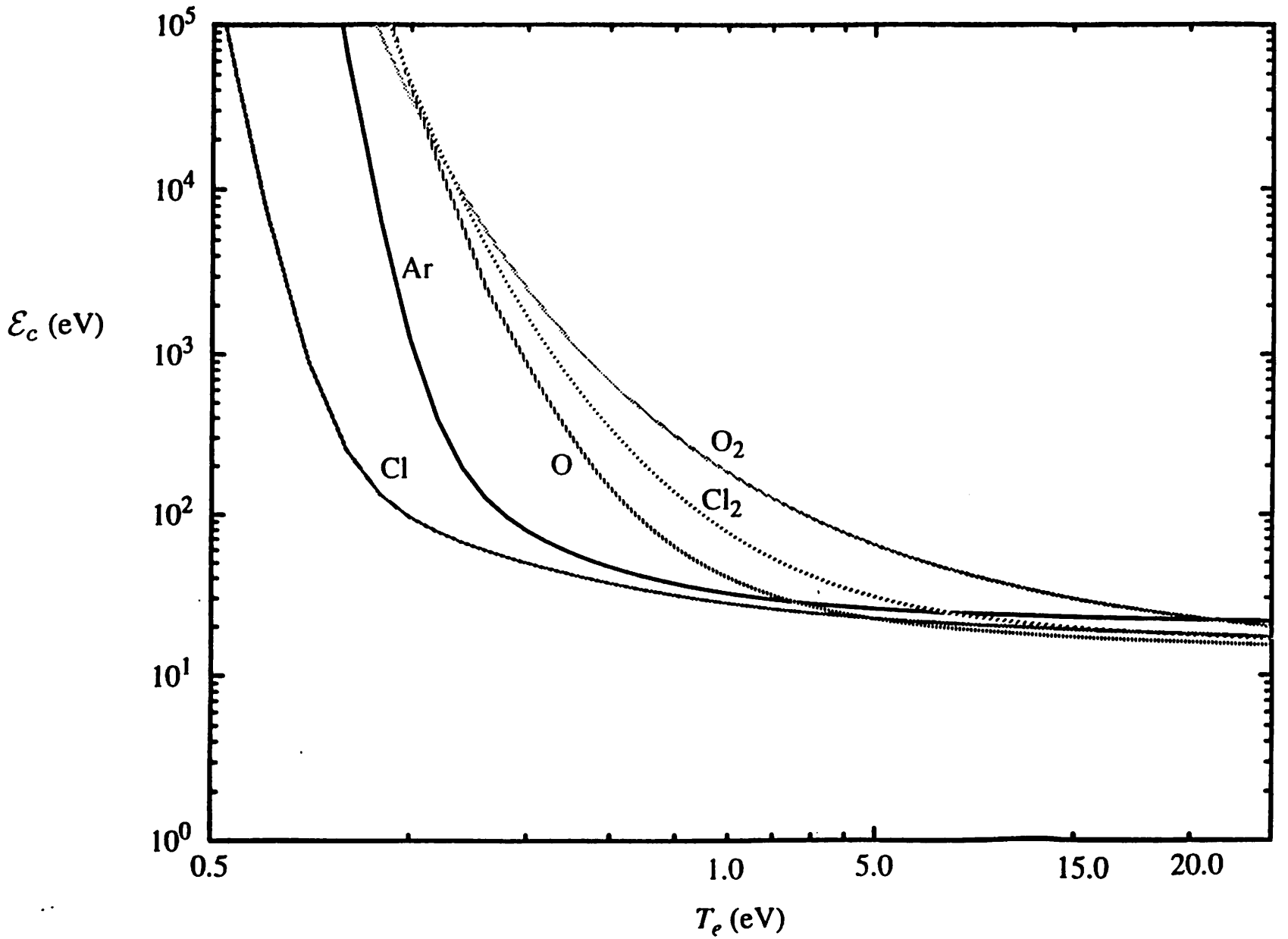
10^5
10^4
10^3
10^2
10^1
10^0
$\mathcal{E}_c$ (eV)
Ar
Cl
O
O_2
Cl_2
0.5
1.0
5.0
15.0
20.0
T_e (eV)

Figure 1

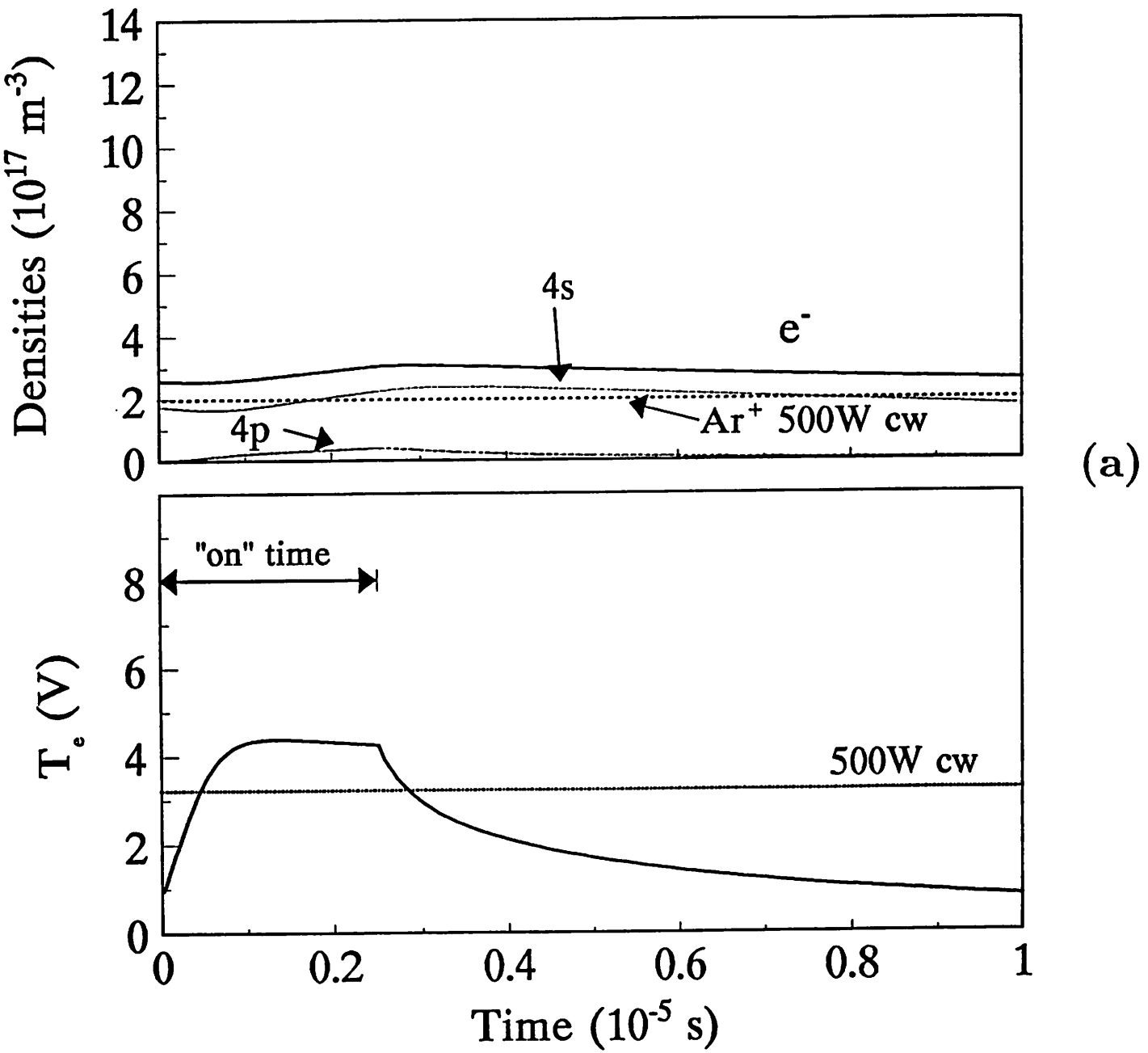
Densities (10^{17} m^{-3})
14
12
10
8
6
4
2
0
4s
e^-
Ar^+ 500W cw
4p
(a)
"on" time
T_e (V)
8
6
4
2
0
500W cw
0
0.2
0.4
0.6
0.8
1
Time (10^{-5} s)

Figure 2a

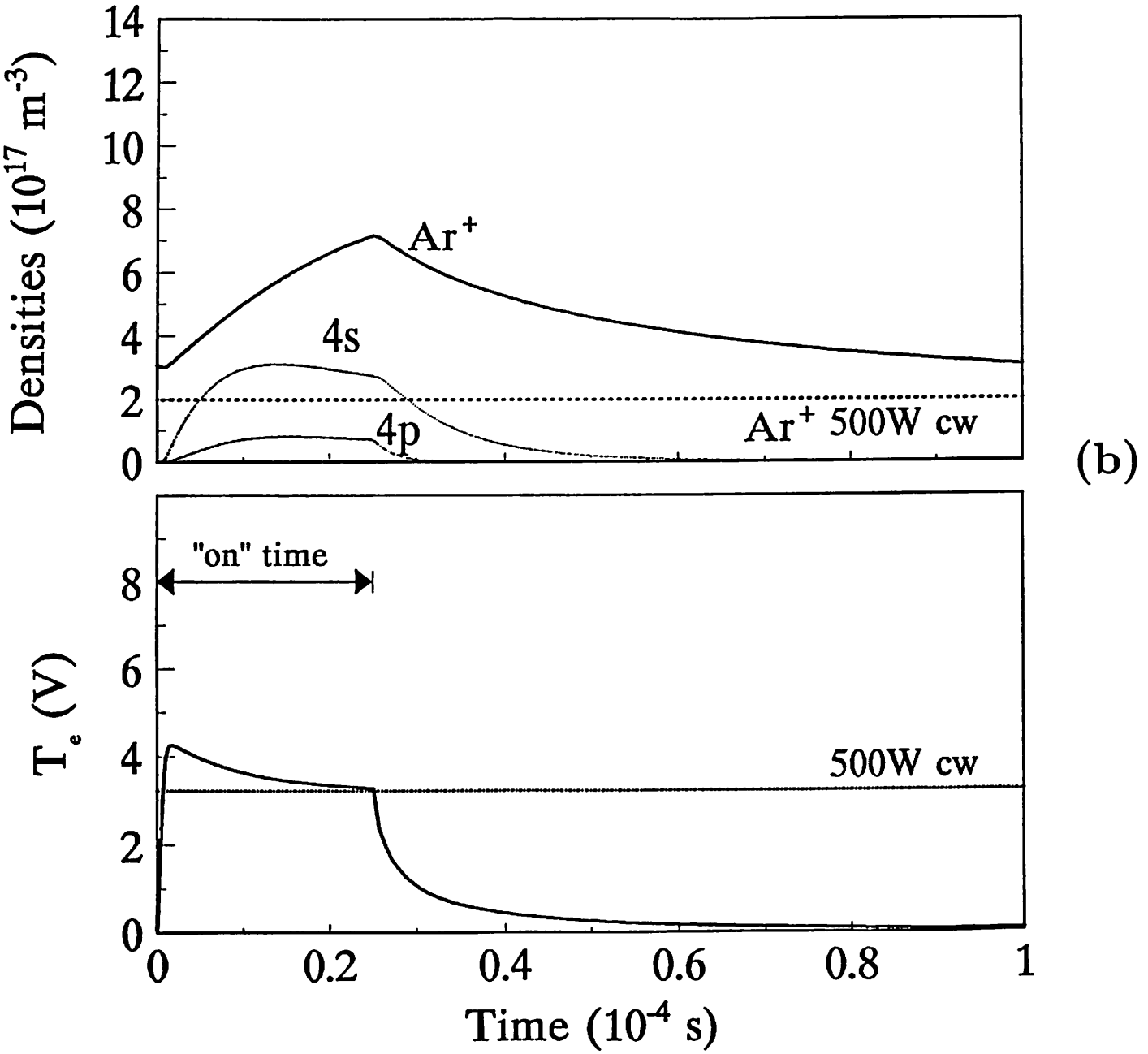
Densities (10^{17} m^{-3})
14
12
10
8
6
4
2
0
Ar$^+$
4s
4p
Ar$^+$ 500W cw
(b)
"on" time
T_e (V)
8
6
4
2
0
500W cw
0
0.2
0.4
0.6
0.8
1
Time (10^{-4} s)

Figure 2b

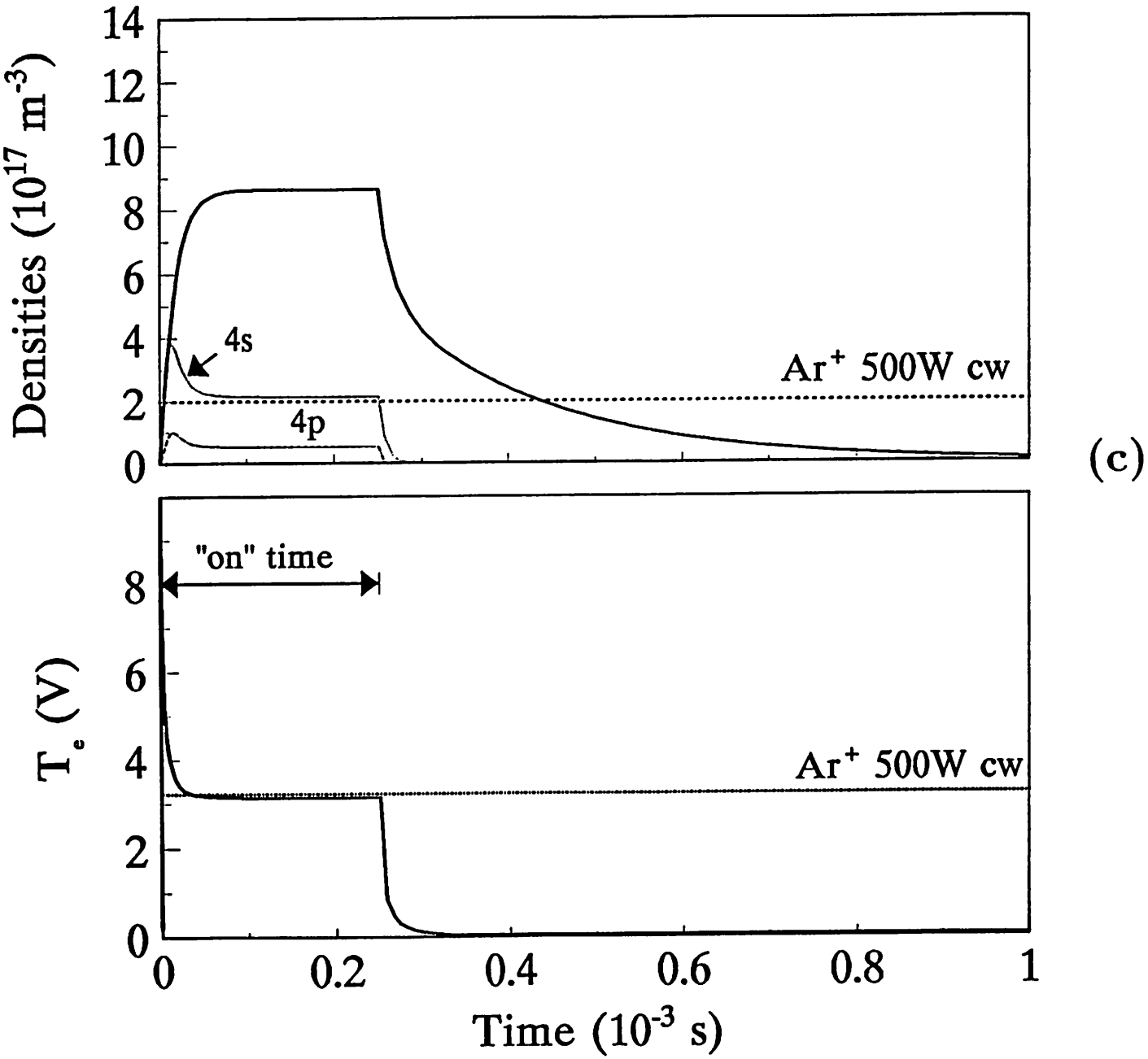
Densities (10^{17} m^{-3})
14
12
10
8
6
4
2
0
4s
4p
Ar^+ 500W cw
(c)
"on" time
T_e (V)
8
6
4
2
0
Ar^+ 500W cw
0
0.2
0.4
0.6
0.8
1
Time (10^{-3} s)

Figure 2c

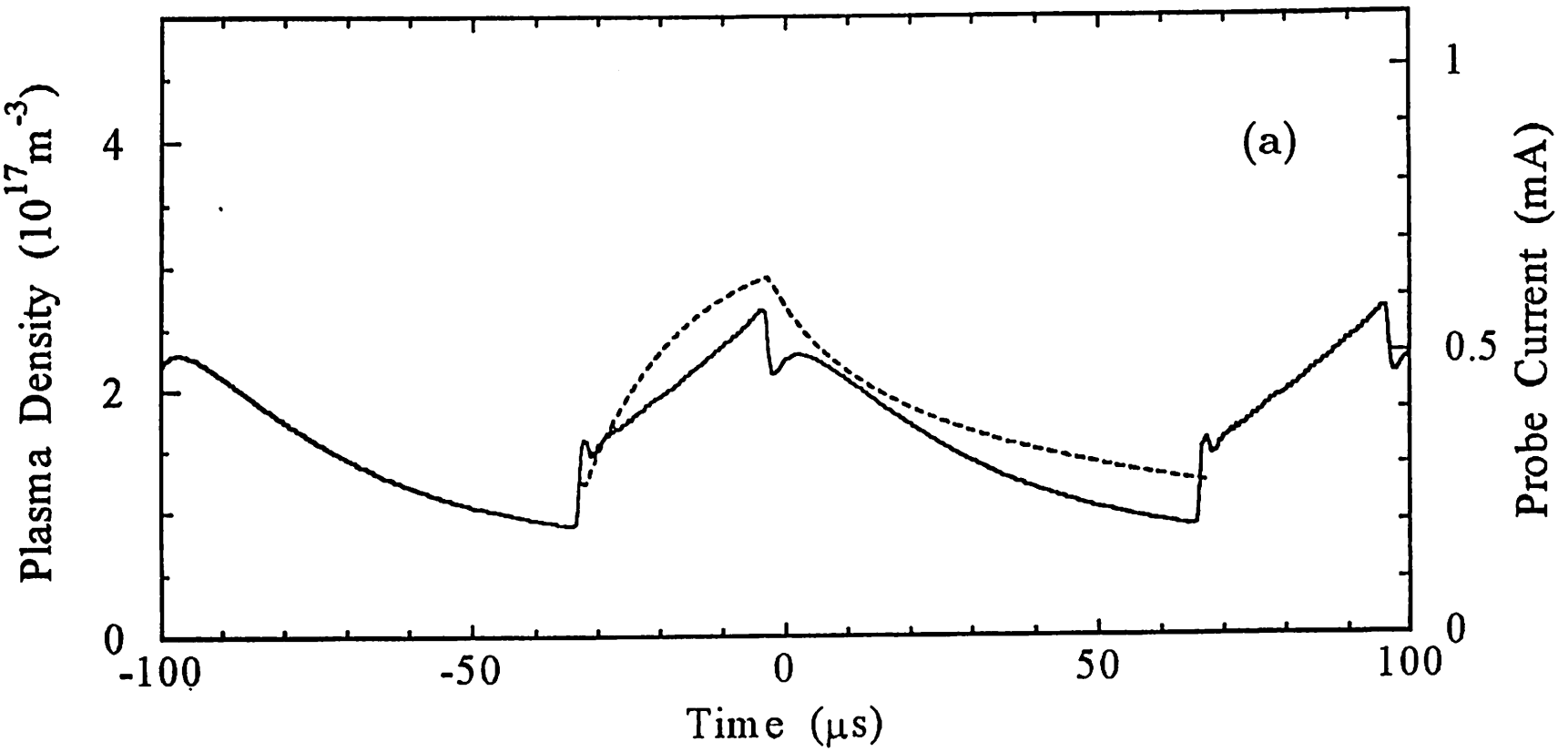
Plasma Density (10^{17}m^{-3})
Probe Current (mA)
(a)
Time (μs)
0
2
4
-100
-50
0
50
100
0
0.5
1

Figure 3a

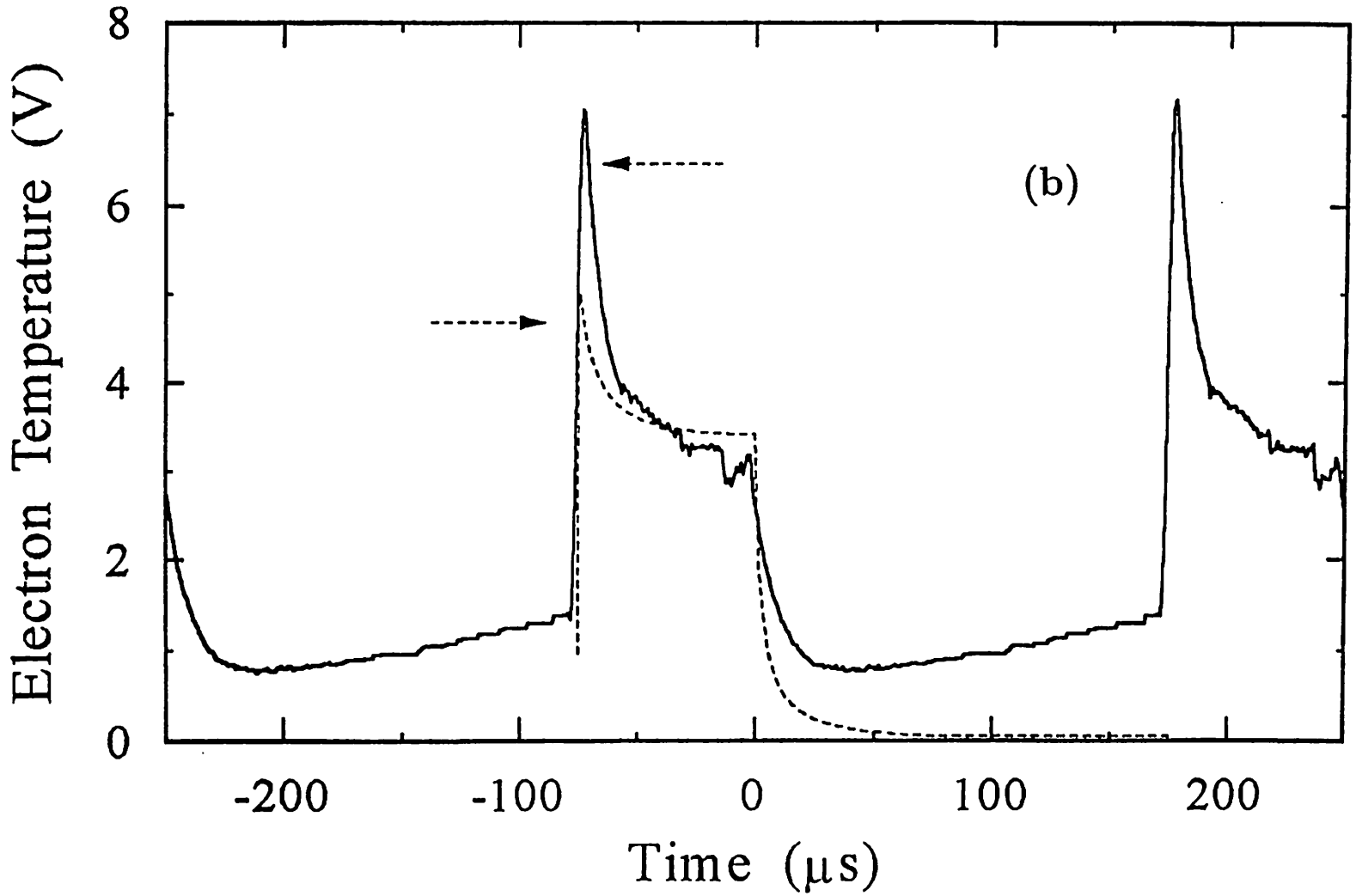

Figure 3b

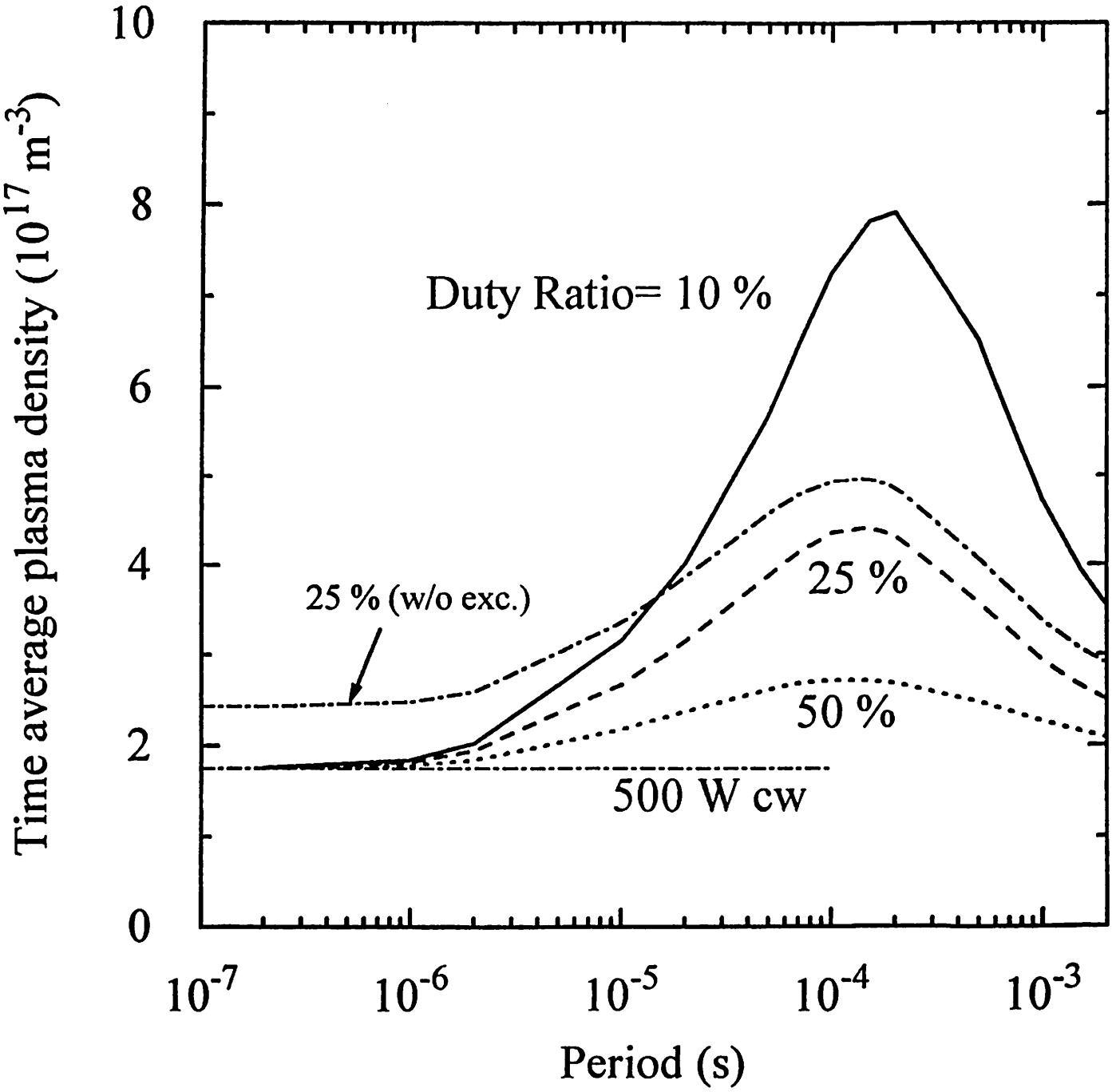
Time average plasma density (10^{17} m^{-3})
10
8
6
4
2
0
Duty Ratio= 10 %
25 % (w/o exc.)
25 %
50 %
500 W cw
10^{-7}
10^{-6}
10^{-5}
10^{-4}
10^{-3}
Period (s)

Figure 4

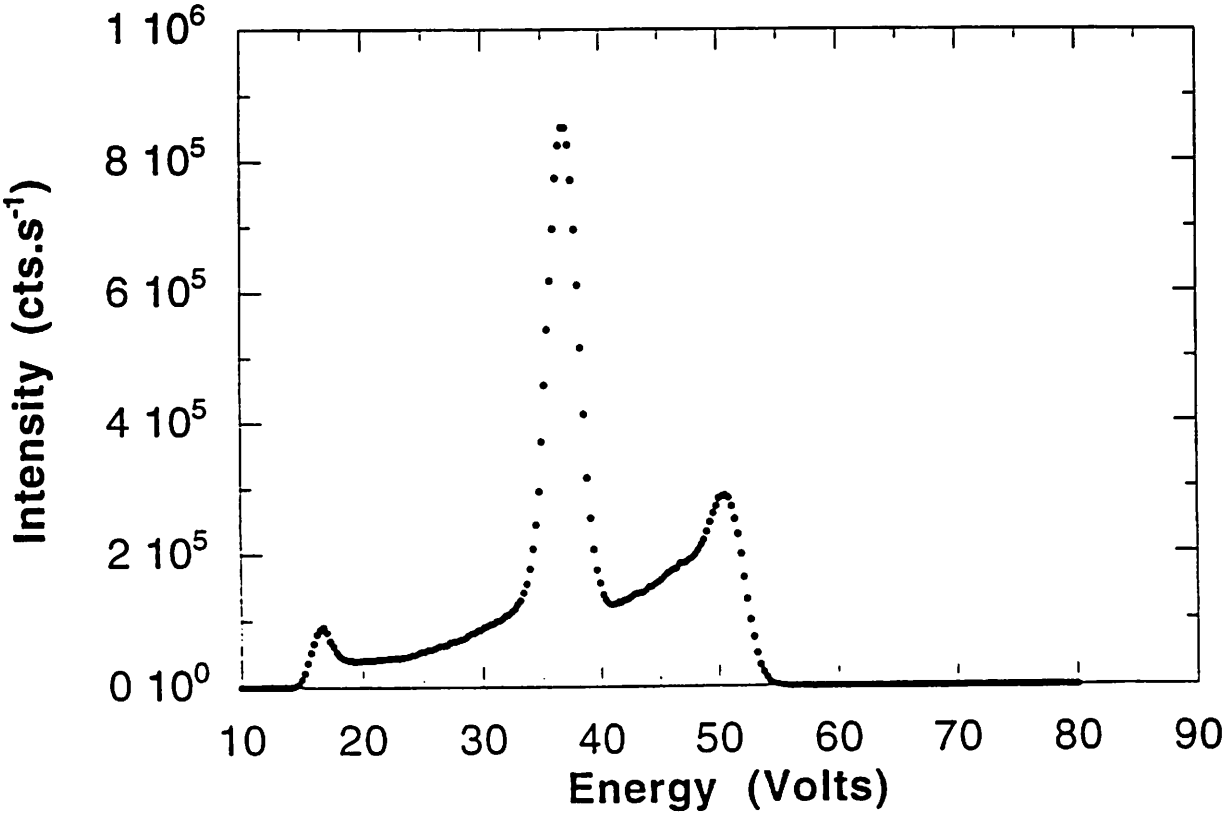
1 10^6
8 10^5
6 10^5
4 10^5
2 10^5
0 10^0
Intensity (cts.s^-1)
10
20
30
40
50
60
70
80
90
Energy (Volts)

Figure 5

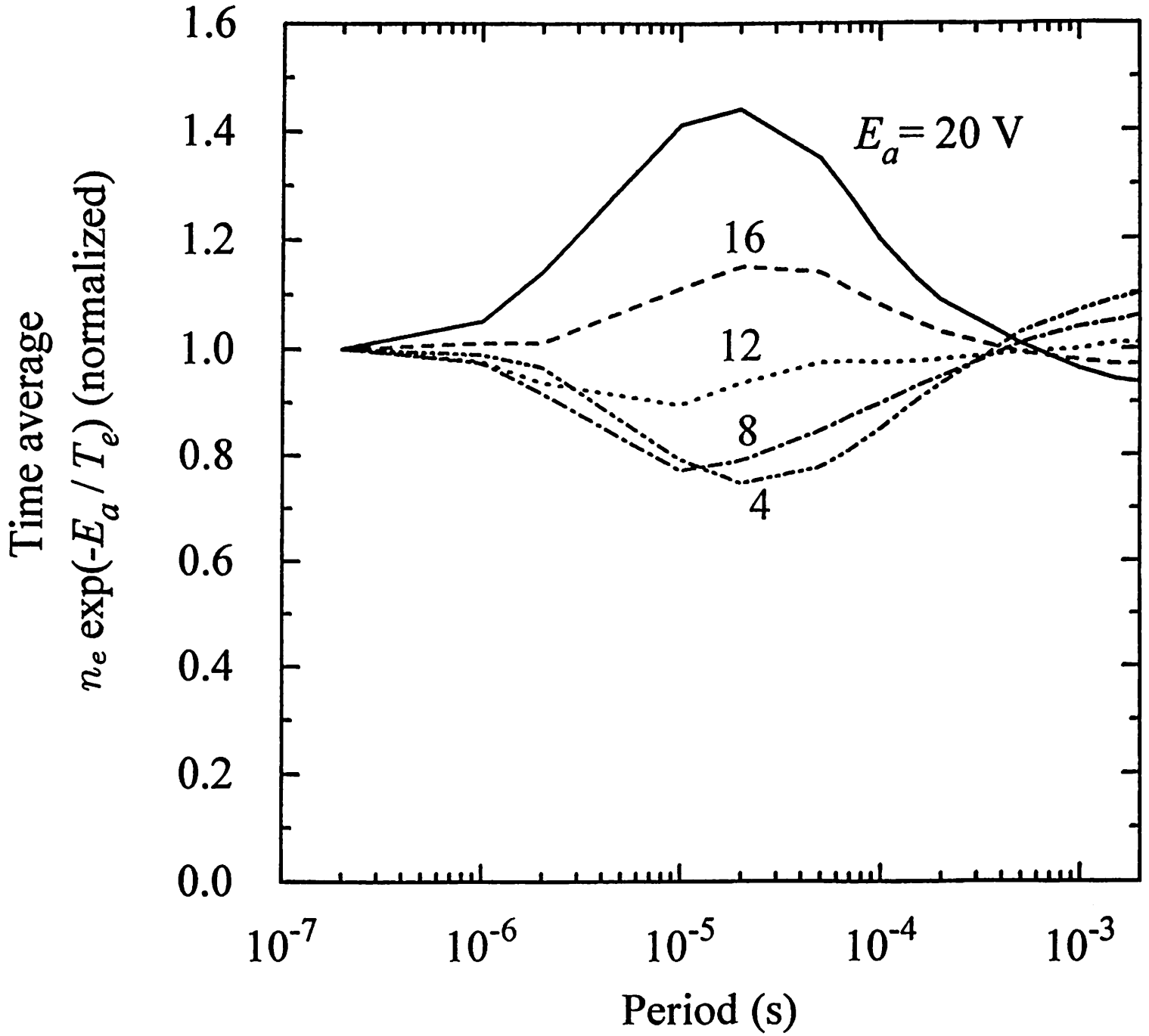
1.6
1.4
1.2
1.0
0.8
0.6
0.4
0.2
0.0
Time average
$n_e \exp(-E_a / T_e)$ (normalized)
$E_a = 20$ V
16
12
8
4
10^{-7}
10^{-6}
10^{-5}
10^{-4}
10^{-3}
Period (s)

Figure 6

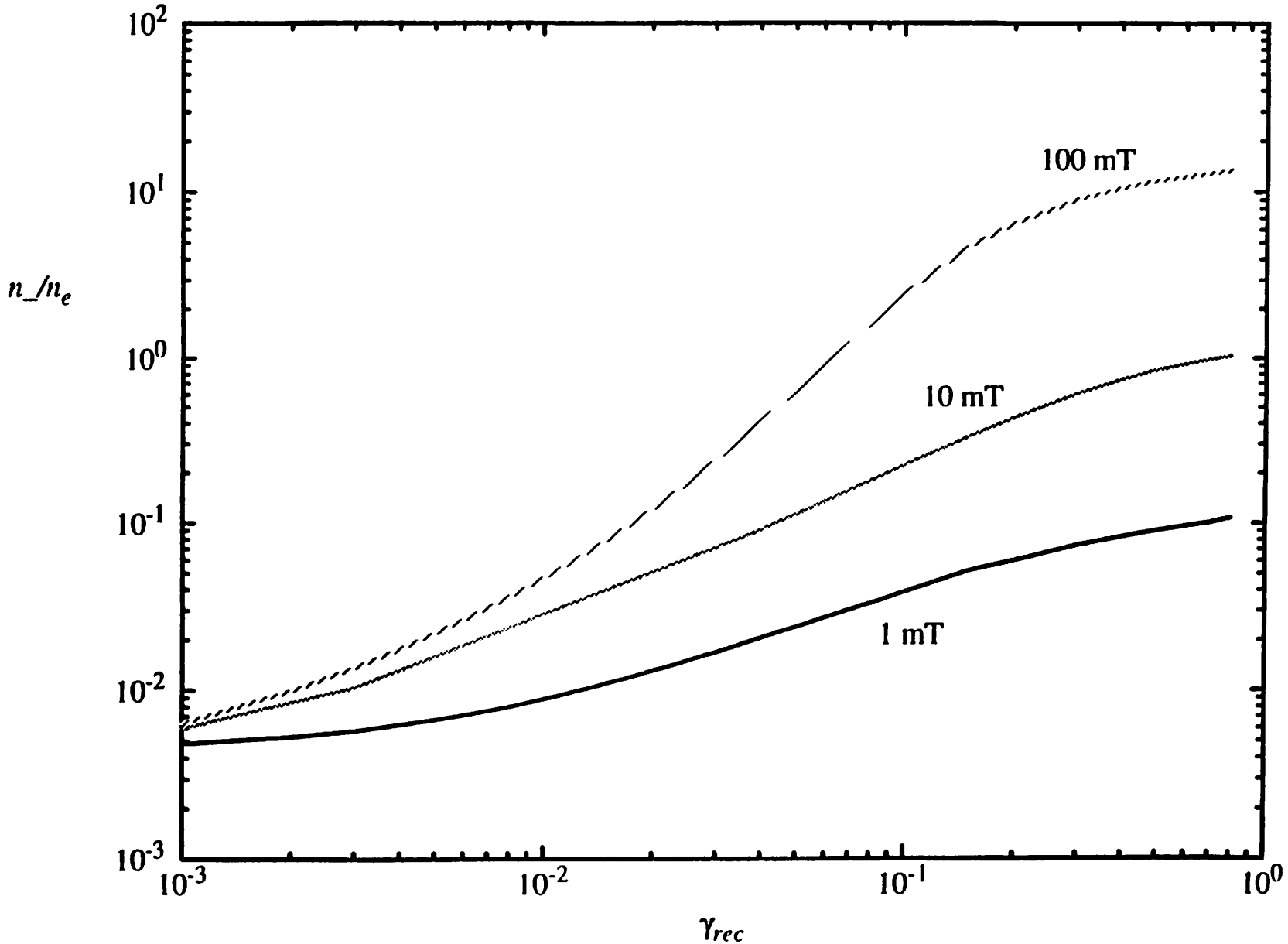
Cl2
10^2
10^1
10^0
10^-1
10^-2
10^-3
n_/n_e
100 mT
10 mT
1 mT
10^-3
10^-2
10^-1
10^0
γ_rec

Figure 7

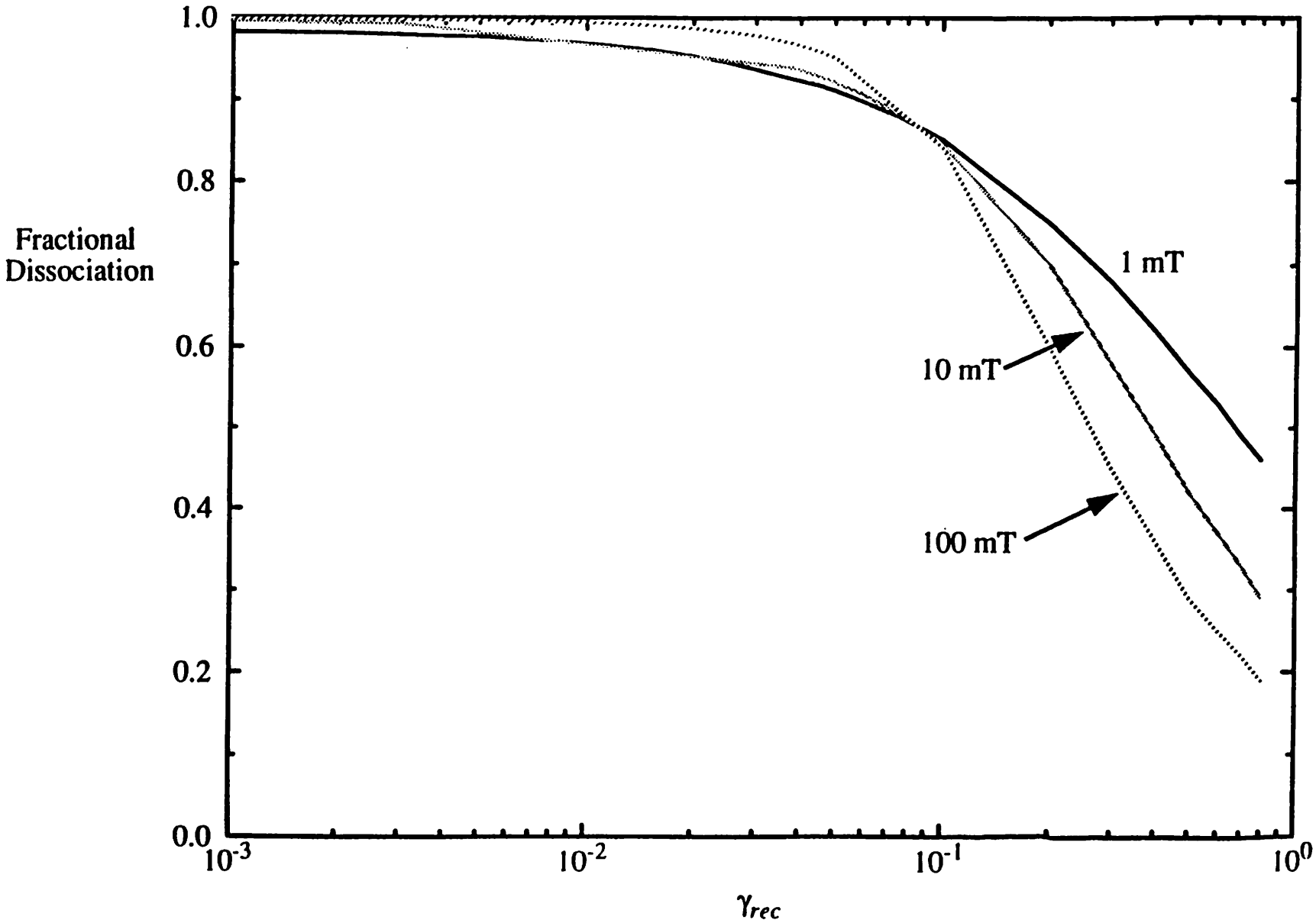
Cl_2
1.0
0.8
0.6
0.4
0.2
0.0
Fractional Dissociation
1 mT
10 mT
100 mT
10^{-3}
10^{-2}
10^{-1}
10^{0}
γ_{rec}

Figure 8

Positive and negative ion densities versus time

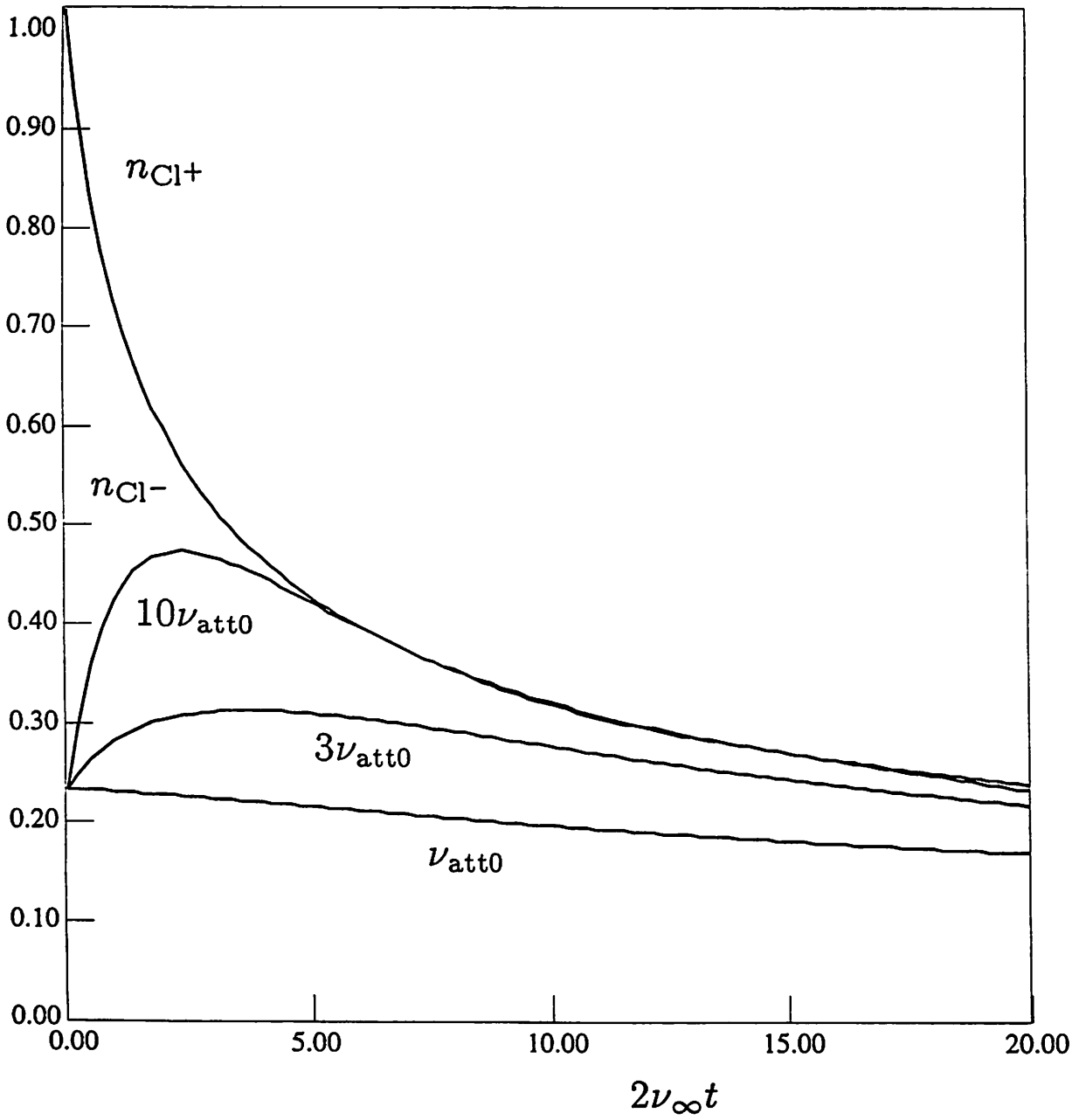

Figure 9

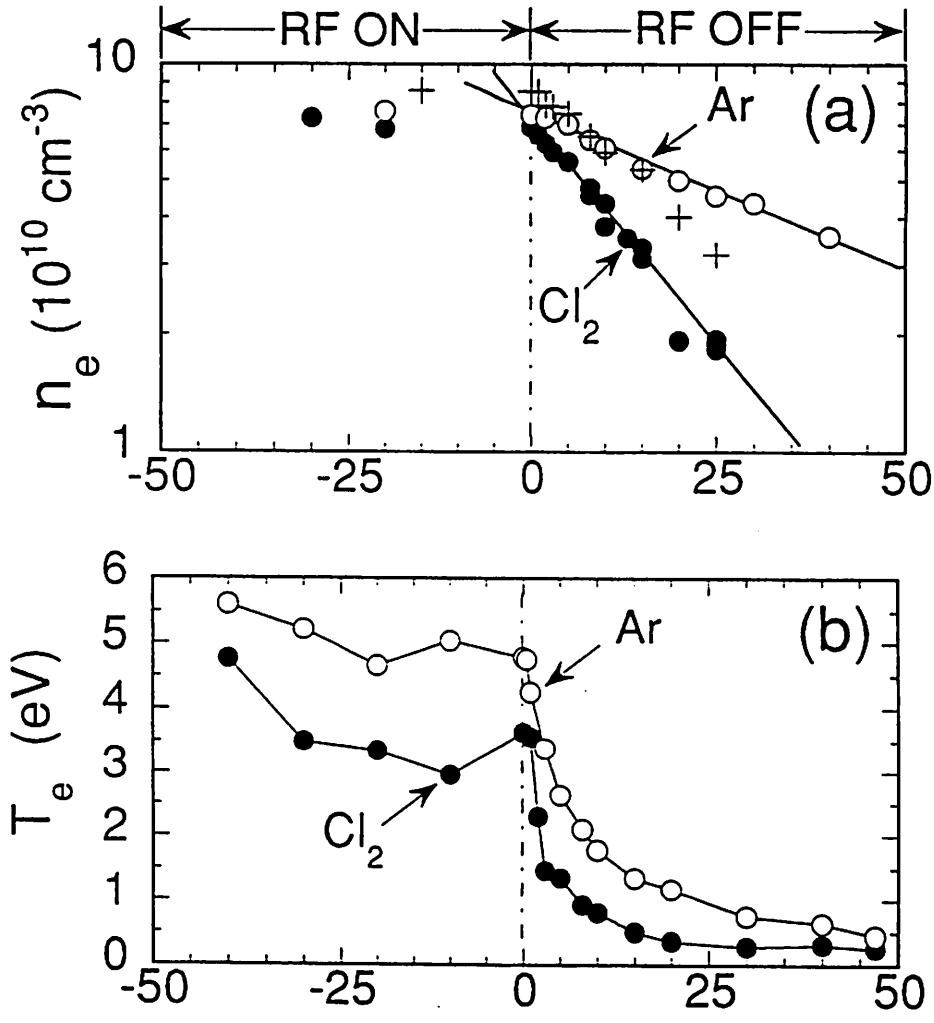
RF ON
RF OFF
10
1
n_e (10^{10} cm^{-3})
Ar
(a)
Cl_2
-50
-25
0
25
50
6
5
4
3
2
1
0
T_e (eV)
Ar
(b)
Cl_2
-50
-25
0
25
50

Figure 10

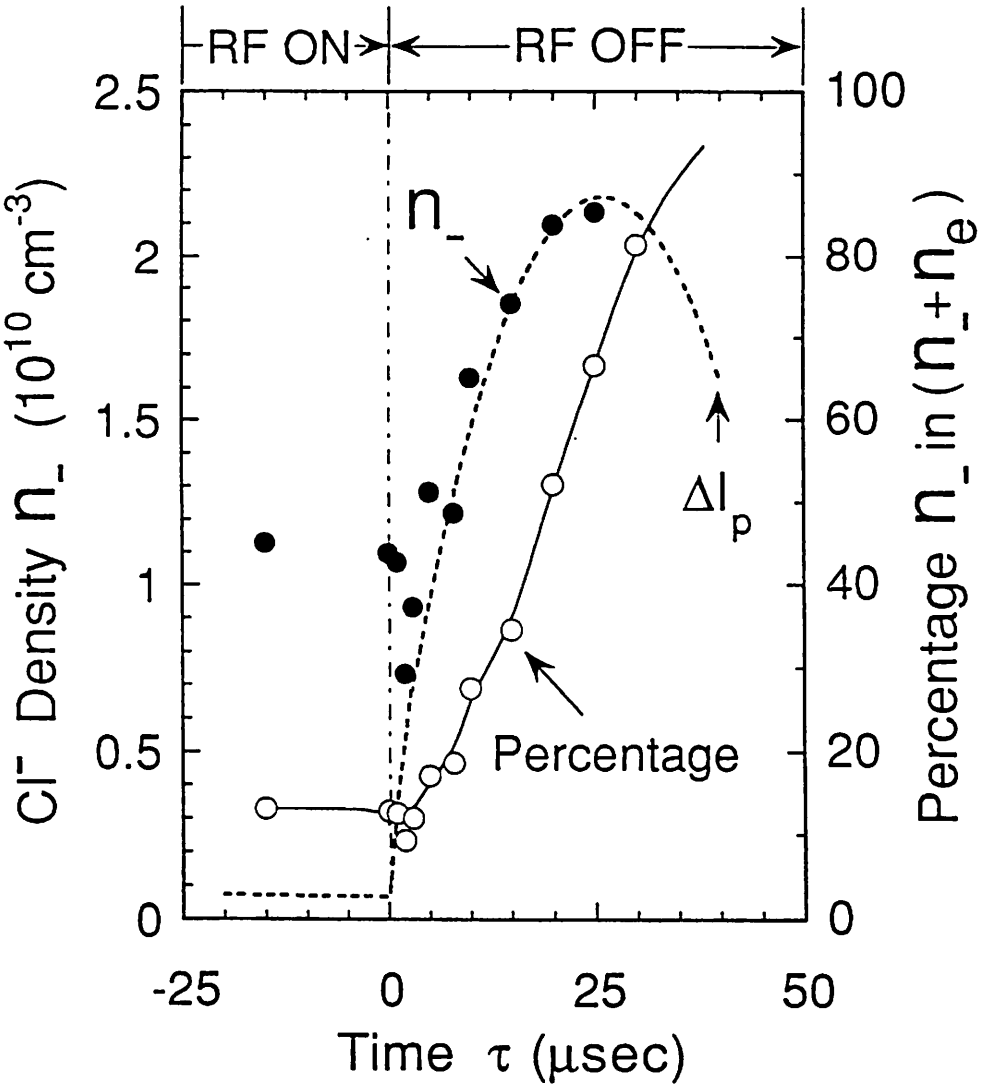
RF ON
RF OFF
2.5
2
1.5
1
0.5
0
100
80
60
40
20
0
-25
0
25
50
n_-
ΔI_p
Percentage
Cl^- Density n_- (10^{10} cm^{-3})
Percentage n_- in (n_-+n_e)
Time τ (μsec)

Figure 11